HAL
open science

The UPR sensor IRE1α promotes dendritic cell responses to control Toxoplasma gondii infection

Anaïs F Poncet, Victor Bosteels, Eik Hoffmann, Sylia Chehade, Sofie Rennen, Ludovic Huot, Véronique Peucelle, Sandra Maréchal, Jamal Khalife, Nicolas Blanchard, et al.

To cite this version:

Anaïs F Poncet, Victor Bosteels, Eik Hoffmann, Sylia Chehade, Sofie Rennen, et al.. The UPR sensor IRE1α promotes dendritic cell responses to control Toxoplasma gondii infection. EMBO Reports, 2021, 22 (3), pp.e49617. 10.15252/embr.201949617 . hal-03286981

HAL Id: hal-03286981

https://hal.science/hal-03286981v1

Submitted on 5 Oct 2021

HAL is a multi-disciplinary open access archive for the deposit and dissemination of scientific research documents, whether they are published or not. The documents may come from teaching and research institutions in France or abroad, or from public or private research centers.

L'archive ouverte pluridisciplinaire **HAL**, est destinée au dépôt et à la diffusion de documents scientifiques de niveau recherche, publiés ou non, émanant des établissements d'enseignement et de recherche français ou étrangers, des laboratoires publics ou privés.

The Unfolded-Protein-Response sensor IRE1α promotes dendritic cell innate immune responses to control *Toxoplasma gondii* infection.

Anaïs F Poncet[1§], Victor Bosteels[2,3§], Eik Hoffmann[1], Sylia Chehade[1], Sofie Rennen[2,3], Ludovic Huot[1], Véronique Peucelle[1], Sandra Maréchal[2,3], Jamal Khalife[1], Nicolas Blanchard[4], Sophie Janssens [2,3*] and Sabrina Marion[1*#]

§ Co-first authors

*Co-senior authors

#corresponding author

[1]Centre d'Infection et d'Immunité de Lille, Université de Lille, INSERM U1019, CNRS UMR 8204, Institut Pasteur de Lille, Lille, France.

[2]Laboratory for ER stress and Inflammation, VIB Center for Inflammation Research, Ghent, Belgium.

[3]Department of Internal Medicine and Pediatrics, Ghent University, Ghent, Belgium.

[4]Centre de Physiopathologie Toulouse Purpan (CPTP), Université de Toulouse, INSERM, CNRS, UPS, Toulouse, France

Key words: UPR, Toxoplasma gondii, dendritic cells, cytokines, antigen presentation.

Abstract

The unfolded protein response (UPR) has emerged as a central regulator of immune cell responses in several physiological and pathologic contexts. However, how intracellular residing pathogens modulate the UPR in dendritic cells (DCs) and thereby affect T cell-mediated immunity remains uncharacterized. Here we demonstrate that infection of DCs by the parasite *Toxoplasma gondii* (*T. gondii*) triggers a unique UPR signature hallmarked by a MyD88-dependent activation of the IRE1α/XBP1s pathway and an inhibition of the ATF6 pathway. Induction of XBP1s controls pro-inflammatory cytokine secretion in infected DCs while IRE1α promotes MHCI antigen presentation of secreted parasite antigens. Also in mice, infection with *T. gondii* leads to a

specific activation of the IRE1α pathway, which was restricted to the cDC1 subset. Mice deficient for IRE1α and XBP1 in DCs display a severe susceptibility to *T. gondii* and succumb during the acute phase of the infection. This early mortality was correlated with increased parasite burden and a defect in splenic T cell responses. Thus, we identify the IRE1α/XBP1s branch of the UPR as a key regulator of host defense responses in DCs upon *T. gondii* infection.

Introduction

Many chronic infections are caused by intracellular microorganisms, which actively manipulate host responses to escape innate immune defenses. There is growing evidence that activation of appropriate antimicrobial activities of infected immune cells relies both on the detection of microbial compounds by Pattern-Recognition-Receptors (PRRs) and on efficient sensing of variations in cellular homeostasis induced by the intracellular pathogen. An essential stress-sensing pathway is the unfolded protein response (UPR). In metazoans, the UPR is activated by the coordinated action of three endoplasmic reticulum (ER) transmembrane sensors: Inositol-Requiring Enzyme 1α (IRE1α), PKR-like ER Kinase (PERK) and Activating Transcription Factors 6α/β (ATF6α/β). The downstream transcriptional programs of the UPR are primarily directed towards restoring proteostasis by increasing ER capacity as well as decreasing protein load, through transient translational inhibition and the process of ER-associated peptide degradation (ERAD) (Walter & Ron, 2011). IRE1α, the most conserved UPR sensor, contains a serine/threonine kinase domain and an endoribonuclease domain. Upon sensing unfolded proteins, IRE1α oligomerizes, is activated by autophosphorylation, and uses its endoribonuclease activity to excise an intron from the transcription factor XBP1 (X-box Binding Protein). This unconventional splicing reaction of the *Xbp1* mRNA generates the active transcription factor XBP1 spliced (XBP1s) (Yoshida *et al*, 2001). In addition to splicing XBP1, upon prolonged or severe stress, IRE1α degrades mRNAs in proximity to the ER in a process termed regulated IRE1-dependent decay (RIDD) of mRNA (Hollien *et al*, 2009). XBP1s and ATF6α up-regulate the expression of genes involved in increasing the protein-folding capacity of the ER (chaperones) as well as ER

62 expansion through phospholipid synthesis (Shoulders *et al*, 2013; Lee *et al*, 2008;
63 Sriburi *et al*, 2007). However, upon irremediable ER stress, the UPR switches to a
64 pro-apoptotic mode by PERK-mediated activation of CHOP expression. During the
65 last decade, a growing number of studies has demonstrated an intricate molecular
66 crosstalk between the immune and UPR pathways, opening new perspectives to
67 treat infections and chronic inflammatory diseases by UPR modulators (Grootjans *et*
68 *al*, 2016; Osorio *et al*, 2018; Reverendo *et al*, 2019). Notably, TLR stimulation of
69 macrophages and dendritic cells (DCs) contributes to XBP1s and CHOP induction that
70 directly activate the transcription of genes encoding pro-inflammatory cytokines,
71 such as IL-6, TNF-α, IFN-β and IL-23 (Cubillos-Ruiz *et al*, 2015; Márquez *et al*, 2017;
72 Martinon *et al*, 2010; Mogilenko *et al*, 2019; Smith, 2018). The IRE1α/XBP1s arm of
73 the UPR is also a key regulator of antigen presentation in DCs via partially
74 characterized mechanisms involving XBP1s-mediated modulation of lipid synthesis
75 (Cubillos-Ruiz *et al*, 2015) and RIDD-mediated regulation of the antigen presentation
76 machinery (Medel *et al*, 2018; Osorio *et al*, 2014, 2018). Several pathogens interfere
77 with the function of the host ER as part of their life cycle, and can selectively activate
78 or repress distinct arms of the UPR (Celli & Tsolis, 2015; Galluzzi *et al*, 2017; Smith,
79 2018). UPR activation can be beneficial to the host by enabling the establishment of
80 an appropriate innate response directed against the invading pathogen (Celli &
81 Tsolis, 2015; Galluzzi *et al*, 2017; Smith, 2018). However, intracellular pathogens can
82 also selectively modulate UPR pathways to promote their own survival and growth.
83 *Toxoplasma gondii (T. gondii)* can be considered as an opportunist parasite as severe
84 symptoms develop in immuno-suppressed patients. However, infection of immuno-
85 competent individuals by type II strains is characterized by bradyzoite-containing
86 cyst development in the brain, leading to life-long chronic infection (Blanchard *et al*,
87 2015). *T. gondii* is a very successful intracellular parasite able to invade any
88 nucleated cells, including immune cells, in which the parasite rapidly replicates
89 within a vacuole. To enable nutrient retrieval from the host and efficient escape
90 from cellular defenses, the parasite secrete numerous effectors that modulate host
91 cell signaling pathways (Hakimi *et al*, 2017). In addition, parasite effectors anchored
92 at the limiting membrane of the vacuole promote recruitment of host organelles,
93 such as mitochondria (Pernas *et al*, 2014, 2018), the Golgi apparatus (Deffieu *et al*,

94 2019) and the ER (Goldszmid *et al*, 2009; Sinai *et al*, 1997). The impact of *T. gondii*
95 induced ER association with the parasitophorous vacuole (PV) on ER homeostasis has
96 not been investigated. Here we demonstrate that infection of DCs by the parasite
97 induces a specific UPR signature, mainly characterized by a MyD88 dependent
98 activation of the IRE1α/XBP1s pathway. In addition, the presence of live parasites
99 actively modulates specific branches of the UPR, in contrast to cell stimulated with
100 heat-killed parasites or soluble *T. gondii* antigens. In infected BMDCs, induction of
101 XBP1s leads to enhanced IL-6 and IL-12 secretion while IRE1α promotes MHCI
102 antigen presentation independently of XBP1s induction. Moreover, activation of the
103 IRE1α/XBP1s pathway in DC is required to promote the establishment of an efficient
104 T cell response and to control parasite dissemination in infected mice.

105 Results

106 *T. gondii* induces IRE1α/XBP1s activation in BMDCs

107 To monitor whether *T. gondii* infection activates the ER stress response, we infected
108 bone marrow derived DCs (BMDCs) with type II Pru parasites for 16h and analyzed
109 IRE1α, PERK and ATF6 pathway activation by measuring the expression of known
110 down-stream targets. As a positive control, we stimulated cells with tunicamycin
111 (TN), a potent pharmacologic ER-stress inducer. In comparison with TN, *T. gondii*
112 infection led to only partial induction of specific UPR branches (Fig 1A and S1).
113 Notably, infection did not induce a classic ER-stress signature as illustrated by the
114 lack of induction of the ER chaperones *Hsp90b1* (encoding GRP94) and *Sec61a1* and
115 the slight induction of *Hspa5* (encoding BIP) compared to TN stimulation (Fig 1A, 1B
116 and S1). On the contrary, the IRE1α branch was induced as illustrated by the
117 increased expression level of *Ern1* (encoding IRE1α) and *Xbp1s* and its target genes
118 *Dnajb9 (*encoding ERdj4) and *Sec24d* (Fig 1A-B and S1). RIDD was not activated, as
119 demonstrated by a lack of degradation of the prototypical RIDD target *Bloc1s1*
120 mRNA upon *T. gondii* infection (Fig 1B) (Bright *et al*, 2015, Hollien *et al*, 2009).
121 Western blot analysis of *T. gondii* infected BMDCs revealed an increasing expression
122 in IRE1α levels with time and the induction of the spliced version of XBP1, which

123 reached its maximal level at 4h (Fig 1C). Sustained activation of IRE1α and transient
124 increase in XBP1s expression was confirmed in so-called Flt3/Notch DCs, an
125 alternative system to generate cDC1s *in vitro* (Kirkling *et al*, 2018) (Fig 1D). The PERK
126 branch appeared not activated, neither at mRNA neither at protein level. PERK
127 down-stream effectors ATF4 and CHOP (encoded by *Ddit3*) were not induced, in
128 contrast to TN stimulation (Fig 1A, 1B and S1). In line with this, phosphorylation of
129 PERK and its target eIF2α appeared decreased compared to steady state levels, and
130 CHOP levels remained undetectable in infected BMDCs and Flt3/Notch DCs (Fig 1C
131 and 1D). As reported before, splenic DCs also display high level of p-eIF2α at steady
132 state suggesting that control of protein translation is essential to regulate DC
133 homeostasis (Clavarino *et al*, 2012). GADD34 interacts with the phosphatase protein
134 1 (PP1) to dephosphorylate eIF2α to alleviate the protein translation block (Clavarino
135 *et al*, 2012; Novoa *et al*, 2001). *Ppp1r15*a (encoding GADD34) gene expression was
136 strongly increased in *T. gondii* infected BMDCs, consistent with a presumable role of
137 GADD34 in the inhibition of eIF2α phosphorylation (Fig 1B). Finally, *T. gondii*
138 infection caused a dramatic down-regulation of the *Atf6* gene and its target gene
139 *Herpud1* (Fig 1A and 1B), suggesting that the parasite actively modulates the ATF6
140 pathway in DCs, as proposed in a previous study (Yamamoto *et al*, 2011). In
141 summary, infection of *T. gondii* leads to a mixed outcome on UPR signaling branches
142 with a down-regulation of the ATF6 branch and an activation of the IRE1/XBP1
143 branch.

144 **Induction of XBP1s is under the control of TLR signaling**

145 UPR activation and down-stream cytokine responses in DCs and macrophages were
146 demonstrated to be under the control of PRR signaling (Martinon *et al*, 2010; Smith,
147 2018). Despite the established role of TLR11/12 in parasite detection in infected
148 mice (Andrade *et al*, 2013; Koblanski *et al*, 2013; Hou *et al*, 2011; Yarovisnki *et al*,
149 2005), the innate sensing mechanisms of parasites residing into a intracellular
150 vacuole are not fully elucidated (Poncet *et al*, 2019) and presumably involve distinct
151 signals depending on early parasite attachment to host cells and subsequent partial
152 vacuolar lysis leading to antigen escape into the host cytosol (Fisch *et al*, 2020;

153 Kongsomboonvech *et al*, 2020; Sardhina-Silva *et al*, 2019, Lee *et al*, 2015). Thus, to
154 establish the role of innate sensing in UPR activation, we used BMDCs differentiated
155 from mice lacking the adaptor MyD88 (MyD88KO mice) (Deguine & Barton, 2014).
156 This adaptor is essential to induce signaling down-stream of all TLRs except for TLR3,
157 which relies on the TRIF adaptor.

158 First, we confirmed that *T. gondii* stimulates the secretion of IL-6 and IL-12 over the
159 time-course of infection (Fig EV1A). In addition, and in contrast to the more virulent
160 type I parasites ("RH" strain), which kill their host prematurely and do not establish
161 latent infections in laboratory mice, type II parasites ("Pru' strain) specifically induce
162 the expression and secretion of IL-23 (Fig EV1B) at a late time point of infection (Fig
163 EV1A), suggesting that distinct innate signaling pathways are involved in the
164 detection of these parasite strains. Lack of MyD88 did not impact on parasite
165 invasion as illustrated by a similar rate of infection between WT and MyD88KO
166 BMDCs (Fig 2A), although we did note a slight alteration in parasite growth (Fig 2B).
167 As expected, absence of TLR stimulation led to a drastic loss of pro-inflammatory
168 cytokine production upon infection (Fig 2C), as revealed by a block in IL-6, IL-12 and
169 IL-23 production. Loss of MyD88 strongly impacted the UPR response in *T. gondii*
170 infected BMDCs. The *T. gondii*-mediated increase in *Xbp1s* and *Dnajb9* expression
171 levels was no longer observed and we even noted a down-regulation of their basal
172 expression level upon infection (Fig 2D). This was also observed for *Ddit3* (encoding
173 CHOP) expression levels when comparing infected versus non-infected conditions
174 (Fig 2D). These results therefore indicate that two separate pathways appear to
175 modulate the host UPR response upon infection with *T. gondii*. TLR signaling is
176 required to induce the IRE1α/XBP1s pathway. In absence of TLR signaling, it
177 becomes obvious that a parasite dependent pathway causes the down-regulation of
178 all UPR branches. Of note, *Ppp1r15a* induction (GADD34) was not dependent on
179 MyD88, suggesting that a distinct MyD88- and PERK-independent signaling pathway
180 induces the expression of this gene during parasite replication (Fig 2D). In line, a
181 previous study demonstrated that GADD34 expression is induced in a IRF3/7-
182 dependent manner after poly:IC stimulation of DCs and controls cytokine production

183 (Dalet *et al*, 2017) (Clavarino *et al*, 2012). Thus, parasite RNA detection following
184 vacuolar lysis could be responsible for GADD34 induction in type II infected DCs.
185 Our results therefore indicate that induction of the IRE1α/XBP1 signaling branch by
186 *T. gondii* infection relies on TLR dependent triggering, confirming earlier studies
187 (Martinon *et al*, 2010).

188 **_T. gondii_ triggers the association of host ER with the parasitophorous vacuole**

189 *T. gondii* actively modulates host cell responses by secreting numerous parasite
190 effectors that highjack host signaling pathways and activate host compartment
191 recruitment at the PV. Notably, host ER (hER) components are recruited in a Sec22b-
192 dependent manner at the PV, a process required to stimulate cross-presentation of
193 soluble secreted OVA antigens by transgenic OVA-expressing parasites (Goldszmid et
194 al, 2009; Cebrian *et al*, 2011). Whether this process impacts on ER homeostasis has
195 never been investigated, nor whether this is needed for triggering of the UPR. First,
196 we quantified hER recruitment in type II Pru parasite infected BMDCs. Electron
197 microscopy analysis showed that almost all the examined PVs (n=116/119) display
198 hER membranes in close association with the PV delimiting membrane (Fig EV2A).
199 Staining of the hER marker KDEL by immunofluorescence confirmed this association
200 (Fig S2A). In addition, this process was also detected in infected human fibroblasts, in
201 which KDEL-positive tubular-like structures were also visualized inside the PV space
202 in close proximity to parasites (Fig S2B). Moreover, we examined hER recruitment in
203 BMDCs incubated with Heat-Killed (HK) parasites that are presumably internalized by
204 phagocytosis or macropinocytosis and do not secrete parasite effectors to modulate
205 host responses. In sharp contrast to live parasite-containing vacuoles, HK-parasite
206 containing vacuoles were never found positive for hER recruitment at their limiting
207 membrane (Fig EV2B). This suggests that hER association with the PV is not specific
208 to immune cells and may be triggered by live parasites to support their survival or
209 replication.

210 **hER recruitment is not required to induce the UPR**

211 In order to determine whether recruitment of the hER to the PV was needed for

212 induction of the UPR, we monitored activation of the UPR and down-stream cytokine
213 responses upon infection of BMDCs by HK *T. gondii*. Similar to live parasites, we
214 found that *Xbp1s* and its down-stream target *Dnajb9* (coding for ERdj4) were
215 induced in BMDCs incubated with HK parasites both at the mRNA and protein levels
216 (Fig EV3A, EV3B and EV3C). However, in sharp contrast to live parasites, the
217 expression of the UPR-induced ER chaperones *Hspa5* (encoding BIP), *Hsp90b1*
218 (encoding by GRP94) and *Sec61a1* was up-regulated as well as the PERK and ATF6
219 pathways (Fig EV3A). Indeed, HK parasites internalization induced the expression of
220 the *Atf4* gene and its target genes *Ppp1r15*a (GADD34) and *Ddit3* (CHOP) as well as
221 *Atf6* (Fig EV3A). However, despite increased in *Ddit3* mRNA levels, we still failed to
222 visualize protein expression in HK parasite stimulated BMDCs (Fig EV3B). This result
223 correlates with previous studies showing that a TRIF-dependent pathway triggered
224 upon TLR stimulation attenuates CHOP translation (Woo *et al*, 2009, 2012). In
225 addition, similar to HK parasites, stimulation of BMDCs with an extract of soluble *T.*
226 *gondii* antigens (STAgs) – which presumably only triggers TLRs - also resulted in the
227 activation of the three branches of the UPR (Fig EV3D and EV3E).
228 Therefore, our results on HK parasite and STAg stimulated BMDCs support the
229 hypothesis that triggering of the IRE1α/XBP1s pathway in infected BMDCs is not
230 dependent on hER recruitment to the PV, but rather relies on TLR dependent
231 signaling.

232 **The presence of replicating parasites modulates the UPR**

233 To further explore a potential modulation of the UPR by replicating parasites, we
234 sorted infected *versus* non-infected bystander BMDCs from a mixed population of
235 infected cells, which included 45% of non-infected cells (Fig 3A) and monitored UPR
236 induction. At 16h post-infection, non-infected bystander BMDCs displayed a
237 significantly higher induction of *Xbp1s* and *Dnajb9* expression compared to infected
238 BMDCs (Fig 3B). These data therefore confirm that parasite invasion/replication is
239 not absolutely required to activate the IRE1α/XBP1s pathway. Furthermore, they
240 also show that the presence of live parasites correlates with a down-regulation of
241 XBP1s induction triggered by TLR stimulation, in agreement with the observed

242 repression of *Xbp1s* monitored in infected MyD88 KO cells compared to non-infected
243 conditions (Fig 2D). Of note, the down-regulation of *Xbp1s, Dnajb9* and *Ddit3*
244 expression in MyD88 KO infected cells was not observed in cells infected with HK
245 parasites (Fig EV4A), further strengthening the hypothesis that secretion of parasite
246 effectors and/or triggering of other signaling pathways upon invasion by live
247 parasites leads to a dampening of UPR host responses. The inhibitory effect seemed
248 to be specific to *Xbp1s* and its down-stream target genes since *Ern1* (encoding
249 IRE1α) expression was comparable in infected and bystander cells (Fig 3B), in line
250 with what we monitored on WB (Fig 1C and 1D). Similarly to the modulation of the
251 IRE1α branch, we also observed an increased expression of the PERK downstream
252 target genes *Atf4* and *Ddit3* in bystander non-infected BMDCs compared to infected
253 BMDCs (Fig 3B). Finally, the down-regulation of the ATF6 target gene *Herpud-1* was
254 no longer observed in bystander infected cells (Fig 3B), suggesting an active down-
255 regulation of the ATF6 branch by parasite derived effector molecules (Fig 3B).

256 In conclusion, the presence of live parasites induces a down-regulation of the UPR
257 triggered by TLR-mediated sensing of parasite compounds.

258 **The IRE1α/XBP1s pathway regulates cytokine response in infected BMDCs**

259 The UPR transcription factors XBP1s and CHOP have been previously demonstrated
260 to regulate cytokine response in TLR-stimulated macrophages (Martinon *et al*, 2010;
261 Smith, 2018) and DCs (Márquez *et al*, 2017; Mogilenko *et al*, 2019). Therefore, we
262 investigated whether *T. gondii*-mediated XBP1s activation impacts on cytokine
263 secretion in infected BMDCs.

264 To establish the function of XBP1s in cytokine production, we used *Xbp1*$^{flox/flox}$Cre-DC
265 mice lacking XBP1 specifically in the CD11c positive cells (hereafter called XBP1ΔDC)
266 (Osorio *et al*, 2014; Tavernier *et al*, 2017). Mice with Xbp1$^{flox/flox}$ alleles but no
267 expression of Cre (hereafter called XBP1$^{fl/fl}$) served as controls for XBP1ΔDC mice
268 (Osorio *et al*, 2014; Tavernier *et al*, 2017). We found that XBP1ΔDC and control
269 BMDCs display a similar rate of infection (Fig 4A and Fig4B) and parasite replication
270 (Fig 4C). However, deletion of XBP1 in *T. gondii* infected BMDCs correlated with a

271 reduced gene expression and protein secretion of IL-6 and IL-12 but not of IL-23
272 when compared to control cells (Fig 4D and Fig 4E). Of note, the decrease in cytokine
273 production was similar at the mRNA and protein levels strongly supporting that
274 XBP1s regulate cytokine expression at the mRNA level. To investigate whether IRE1α
275 also contributes to the regulation of cytokine secretion, we used XBP1ΔDC
276 IRE1α^{trunc}DC mice. These mice were obtained by crossing XBP1ΔDC mice with *Ern1*$^{fl/fl}$
277 mice that bear loxP sites flanking exon 20 and 21 of the *Ern1* gene (encoding IRE1α)
278 (Tavernier *et al*, 2017). DCs from XBP1ΔDC IRE1^{trunc}DC mice are deficient for XBP1
279 and harbor a low expressed truncated IRE1α isoform with impaired endonuclease
280 activity. Of note, as previously described (Medel *et al*, 2018), GM-CSF differentiated
281 BMDCs display strongly reduced but not fully abrogated IRE1α expression (Fig EV5A).
282 We did not measure further decrease in IL-6, IL-12 or IL-23 secretion in XBP1ΔDC
283 IRE1^{trunc}DCs indicating that *T. gondii*-induced XBP1s induction selectively contributes
284 to cytokine production in infected BMDCs upon activation of IRE1α (Fig 4D and 4E).
285 Importantly, the defect in cytokine production monitored in XBP1ΔDC BMDCs and
286 XBP1ΔIRE1^{trunc}DC BMDCs was not a result of cell death induced upon infection or
287 impaired differentiation as illustrated by a similar percentage of CD11c^{+}/MHCII^{+}
288 positive cells (Fig EV5B). Additionally, XBP1ΔDC BMDCs and XBP1ΔIRE1^{trunc}DC BMDCs
289 displayed similar surface expression levels of the co-stimulatory molecules CD80 and
290 CD86 upon LPS stimulation (Fig EV5C) indicating that deletion of XBP1 and IRE1α did
291 not impact on BMDCs activation upon immunogenic stimulation. Moreover, similar
292 to BMDCs invaded by live parasites, XBP1ΔDC BMDCs incubated with HK parasites
293 displayed a drastic inhibition in the gene expression and protein secretion of IL-6 and
294 IL-12 (Fig EV6A and EV6B), further supporting the hypothesis that the IRE1α/XBP1s
295 pathway is triggered in a TLR-dependent manner to regulate cytokine production. Of
296 note, in contrast to IL-6 and IL-12, IL-23 was less induced by HK parasites, suggesting
297 that the presence of live parasites is required to trigger production of this cytokine
298 (Fig EV6). However, the production of all cytokines induced by HK parasites was fully
299 dependent on TLR/MyD88 signaling (Fig EV4B).

300 Collectively these data demonstrate that upon *T. gondii* infection of BMDCs, IL-6 and
301 IL-12 secretion is partially under the control of IRE1α/XBP1s signaling activated via

302 MyD88. In contrast, IL-23 production is IRE1α/XBP1s-independent, requires live
303 parasite invasion, and is only partially dependent on MyD88 signaling.

304 **The IRE1α/XBP1s pathway regulates cross-presentation of soluble secreted**
305 **parasite antigens**

306 Several studies reported the implication of the IRE1α branch of the UPR in regulating
307 MHCI antigen presentation in DCs both at steady-state and in activated conditions
308 (Osorio *et al*, 2018). Activation of the IRE1α/XBP1s axis was found to have beneficial
309 or detrimental outcomes on T cell activation depending on the nature of the
310 stimulation and the antigen. Notably, in the context of tumors, reinforcing XBP1s
311 expression ameliorates cross-presentation and priming of $CD8^+$ T cells (Zhang *et al*,
312 2015). Similarly, the inhibition of IRE1α endoribonuclease activity in cDC1 leads to
313 reduced soluble melanoma antigen cross-presentation to $CD8^+$ T cells but has no
314 impact on MHCII antigen presentation (Zhang *et al*, 2015). So far, the implication of
315 the IRE1α/XBP1s pathway in MHCI antigen presentation has not been addressed in
316 the context of DCs infected by intracellular pathogens. To address this question, we
317 infected BMDCs with type II parasites expressing the soluble model antigen OVA,
318 which is secreted in the vacuolar space of the PV. MHCI presentation of this antigen
319 has been previously demonstrated to depend on hER component recruitment at the
320 PV, notably TAP and the translocon Sec61 (Cebrian *et al*, 2011; Goldszmid *et al*,
321 2009; Gubbels *et al*, 2005). We used LacZ-inducible reporter CD8 T cell hybridomas
322 (B3Z) that specifically respond to H-$2K^b$-SIINFEKL complexes to assess secreted OVA
323 presentation by control $XBP1^{fl/fl}$ $IRE1^{fl/fl}$, XBP1ΔDC and XBP1ΔDC $IRE1\alpha^{trunc}$DC BMDCs.
324 Since XBP1ΔDC $IRE1\alpha^{trunc}$DC may display residual IRE1α activity (Fig EV5A), we
325 additionally treated control cells with 4μ8C, a selective and potent inhibitor of the
326 IRE1α endoribonuclease domain as illustrated by the complete inhibition of *Xbp1s*
327 induction and its target *Dnajb9* upon infection or treatment with tunicamycin (Fig
328 S3A and S3B). 4μ8C treatment also inhibited IL-6 and IL-12 secretion (but not IL-23
329 production) induced upon infection (Fig S3C) similarly to what we observed in
330 XBP1ΔDC and XBP1ΔDC $IRE1\alpha^{trunc}$DC BMDCs (Fig 4D).
331 We found that inhibition of IRE1α by 4μ8C results in a pronounced decrease in

332 SIINFEKL (SKL8) peptide presentation by infected cells (Fig 4F). A significant inhibition
333 of SKL8 peptide presentation was also observed in XBP1ΔDC IRE1α^{trunc}DC BMDCs (Fig
334 4F), although less pronounced, which may reflect the partial deletion of IRE1 in in
335 these cells. Interestingly, XBP1ΔDC infected BMDCs were not inhibited in SKL8
336 peptide presentation demonstrating that this process is not dependent on XBP1s
337 induction (Fig 4F). The defect in SKL8 peptide presentation observed in XBP1ΔDC
338 IRE1α^{trunc}DC was not due to altered parasite infection (Fig 4G) or to reduced MHCI
339 surface expression (Fig 4H and 4I), also supported by similar exogenous presentation
340 of the SKL8 peptide in all studied conditions (Fig 4H). In conclusion, our data indicate
341 that IRE1α but not XBP1s contributes to CD8^{+} T cell priming by *T. gondii* secreted
342 antigens in BMDCs.

343 **The IRE1α pathway is stimulated in splenic cDC1 during infection**

344 To assess whether the IRE1α pathway is activated during *T. gondii* infection of mice,
345 we used ERAI reporter mice (Iwawaki *et al*, 2004). These mice express a partial
346 sequence of human XBP1 fused to Venus fluorescent protein (VenusFP) that includes
347 the sites at which IRE1α splices XBP1 (Iwawaki *et al*, 2004). Thus, detection of the
348 VenusFP signal in cells allows reporting of IRE1α activation. Our previous findings
349 demonstrated a preferential induction of the IRE1α arm of the UPR in basal-state
350 splenic cDC1 over cDC2 and pDC (Osorio *et al*, 2014; Tavernier *et al*, 2017). ERAI and
351 control mice were infected with a low dose of Pru parasites and the different
352 subpopulations of splenic DCs were analyzed 6 days post-infection by flow
353 cytometry.
354 In line with our previous findings, a VenusFP signal was detected at steady state in
355 cDC1s (CD26^{+}/CD11c^{hi}/MHCII^{hi}/XCR1^{+}/CD172a^{-}) but not in cDC2s
356 (CD26^{+}/CD11c^{hi}/MHCII^{hi}/XCR1^{-}/CD172a^{+}) (Fig 5A, 5B and 5C). Upon infection, the
357 VenusFP signal greatly increased in the cDC1 subset while it remained unchanged in
358 the cDC2 population (Fig 5A, 5B and 5C) indicating that IRE1α activation and
359 subsequent XBP1s expression is restricted to cDC1s. We also did not monitor
360 substantial XBP1s induction in splenic neutrophils, monocytes, B and T cells
361 suggesting that the UPR contributes to the regulation of cDC1 functions upon *T.*

362 *gondii* infection (Fig 5D and S4A). To further confirm these results, we sorted splenic
363 cDC1s and cDC2s from 6 days WT infected mice and examined UPR induction by
364 quantifying the mRNA levels of different UPR targets. Consistent with the results
365 obtained in ERAI mice, a strong up-regulation of *Ern1* (IRE1α) and *Xbp1s* transcripts
366 were monitored only in cDC1s but not in cDC2s. The expression of the PERK target
367 *Ddit3* (CHOP) was not induced in none of the cDC sub-types (Fig 5E and 5F).
368 Importantly, similar to observations made in previous studies (John *et al*, 2009), the
369 percentage of dTomato-positive infected cells was very low in the spleen of ERAI
370 infected mice suggesting that parasite invasion and replication may not be required
371 to trigger the massive activation of the IRE1α pathway monitored in cDC1s (Fig S4B).
372 This hypothesis correlates with our *in vitro* findings indicating that induction of
373 XBP1s in BMDCs is dependent on innate sensing of particulate antigens and does not
374 require parasite invasion.

375 **IRE1α/XBP1s pathway activation plays an essential protective role against *T. gondii***
376 **infection**

377 To determine the contribution of DC-specific activation of IRE1α in the resistance to
378 *T. gondii* infection, we assessed the survival rate of control XBP1$^{fl/fl}$ IRE1α$^{fl/fl}$ mice
379 compared to XBP1ΔDC IRE1α^{trunc}DC mice injected intraperitoneally with Pru
380 parasites. Our data showed that XBP1ΔDC IRE1α^{trunc}DC mice were highly susceptible
381 to infection when compared to control mice and all succumbed between 9 and 12
382 days post infection (Fig 6A). This result indicates that activation of the IRE1α
383 pathway in DCs plays an essential protective role against *T. gondii* acute infection. To
384 gain insights into the processes leading to XBP1ΔDC IRE1α^{trunc}DC mice early
385 mortality, we isolated splenocytes and cells from the peritoneal exudate (PEC) of
386 infected mice and analyzed parasite load by qPCR. We found a significant increase in
387 parasite burden in both organs in XBP1ΔDC IRE1α^{trunc}DC mice compared to control
388 mice, indicating an altered parasite control (Fig 6B). We did not detect any significant
389 changes in *Il-12* expression in the spleen of infected XBP1ΔDC IRE1α^{trunc}DC mice,
390 presumably due to the contribution of other splenic cell types, notably cDC2s and
391 monocytes, in the secretion of this cytokine (Fig 6C). However, a reduced *Ifng* and

392 *Tnfα* expression was monitored in XBP1ΔDC IRE1α^{trunc}DC mice compared to control
393 mice suggested a defect in T cell activation that could be caused by cDC functional
394 alteration in antigen presentation (John *et al*, 2009; Lee *et al*, 2015). Accordingly,
395 while in control mice, CD4 T and CD8 T cell showed increased proliferation upon
396 infection, this expansion was not observed in XBP1ΔDC IRE1α^{trunc}DC mice (Fig 6D and
397 6E). We also noticed a defect in CD8 T cell activation as noted by the decreased
398 number of IFNγ-expressing CD8 T cells but not of IFNγ-expressing CD4 T cells,
399 suggesting an alteration of cross-presentation by cDC1 (Fig 6D and 6E). Finally, we
400 observed that the number and frequency of splenic cDC1s and cDC2s both increased
401 upon infection of WT mice (Fig 6F). On the contrary, XBP1ΔDC IRE1α^{trunc}DC mice,
402 which exhibit a similar number of the two cDC subsets at steady-state compared to
403 control mice, do not show increased cDC1s number and frequency upon infection
404 (Fig 6F). This defect was not observed for cDC2s, consistent with a specific activation
405 of the IRE1α pathway in cDC1s (Fig 5A and 5B) and a defect in CD8 T cell activation
406 (Fig 6E). These data therefore suggest that the IRE1α pathway, may not only regulate
407 cross-presentation to CD8 T cells but also promote the expansion of the cDC1 subset
408 triggered upon infection.

409

410 **Discussion**

411 Very few studies addressed the impact of UPR signaling in DCs in response to
412 infection by an intracellular pathogen. Our results demonstrate that infection of
413 BMDCs by *T. gondii* specifically activated the IRE1α/XBP1s branch, while the PERK
414 pathway was not activated and the ATF6 branch even repressed. Experiments
415 comparing infected *versus* non-infected bystander BMDCs, or heat-killed *versus* live
416 parasites revealed that triggering of the UPR does not require active invasion with
417 live parasites, but relies on TLR-mediated sensing of parasite compounds (Figure 7A).
418 On the other hand, secretion of parasite effectors and/or triggering of other
419 signaling pathways upon invasion by live parasites leads to a dampening of the UPR,
420 which is especially prominent for the ATF6 and PERK branch (Figure 7B).
421 Manipulation of the UPR has been well documented during viral infections (Smith,

422 2018). For instance, the chikungunya virus shuts-down the PERK pathway to sustain
423 eIF2α-mediated translation of viral proteins and to avoid CHOP-induced apoptosis of
424 the host cell, but activates the IRE1α and ATF6 pathways to enhance ER capacity
425 (Rathore *et al*, 2013). Similarly, we found that the presence of live parasites led to a
426 down-regulation of the UPR triggered by TLR stimulation. Along these lines, it has
427 been reported that *Tg*ROP18, a parasite effector anchored at the limiting membrane
428 of the vacuole phosphorylates ATF6β, leading to its degradation via the proteasome
429 (Yamamoto *et al*, 2011). Our data indicate that the ATF6 pathway is also repressed at
430 the transcriptional level in infected BMDCs by yet unknown mechanisms. Also ATF4
431 and CHOP, downstream mediators of the PERK pathway were not induced in
432 infected BMDCs. TLR stimulation has been previously shown to correlate with a TRIF-
433 dependent attenuation of CHOP translation as we also noted in HK or STAg-
434 stimulated parasites (Woo *et al*, 2009, 2012). However, infection with live parasites
435 led to repression of CHOP already at the transcriptional level, which became
436 apparent upon comparison of WT *versus* MyD88KO cells. This process may allow the
437 infected host cell to avoid CHOP-induced apoptosis.
438 The mechanisms by which infection by live parasites modulates the UPR remain to
439 be elucidated. To escape cellular defenses, *T. gondii* secretes numerous parasite
440 effectors that modulate host cell signaling pathways (Hakimi *et al*, 2017). In addition,
441 parasite effectors anchored at the limiting membrane of the vacuole promote
442 recruitment of host organelles, most likely to stimulate host lipid uptake required to
443 endure the successive divisions of this fast replicating parasite. *T. gondii* stimulates
444 the recruitment of mitochondria (Pernas *et al*, 2014, 2018), fragmented Golgi
445 (Deffieu *et al*, 2019), endosomes (Romano *et al*, 2017) and the hER (Goldszmid *et al*,
446 2009; Sinai *et al*, 1997). It is likely that sensing mechanisms detect changes in
447 organelle structure and functions, which result in the stimulation of specific
448 downstream responses. In support of this hypothesis, the transcriptional response of
449 cells invaded by TgMAF-1-deficient parasites, which are unable to recruit
450 mitochondria at the PV, revealed major changes in cytokine responses (Pernas *et al*,
451 2014). By contrast to mitochondria and Golgi vesicles, the effectors that stimulate
452 hER association with the PVM are not identified. A previous work reported the
453 interaction of *Tg*GRA3 with calcium modulating ligand (CAMLG), a type II

454 transmembrane protein of the ER, but demonstration of a functional role of *Tg*GRA3
455 in this process is lacking (Kim *et al*, 2008). As previously observed by others, we
456 detected hER association with the PV in fibroblasts and BMDCs infected with type II
457 Pru parasites but this process was not required to induce the UPR. However, hER
458 recruitment by the parasite may contribute to the modulation of the UPR pathways
459 induced by TLR-stimulation. Thus, identification of the parasite effectors contributing
460 to hER recruitment at the PV would allow exploring its impact on the regulation of
461 hER functions, the possible modulation of the UPR and down-stream innate immune
462 responses. In general, further characterization of the induced UPR pathways in DCs
463 infected with parasites deficient in the secretion of parasite effectors (Franco *et al*,
464 2016; Naor *et al*, 2018; Panas *et al*, 2019) will also help to identify the mechanisms
465 by which *T. gondii* modulates the UPR.
466
467 Also *in vivo,* infection with live parasites appeared not essential to trigger the UPR in
468 DCs, as non-infected bystander rather than infected DCs showed activation of the
469 IRE1α branch. Indeed, while activation of IRE1α in splenic cDC1 was high at day 6
470 post-infection, the level of infected cells at that moment was very low, although
471 parasite DNA was still clearly detected by qPCR. This is consistent with the study of
472 John et al. suggesting that cross-presentation by bystander DCs rather than infected
473 DCs is an important route of antigen presentation during toxoplasmosis (John *et al*,
474 2009). Along these lines, it has been demonstrated that during influenza virus
475 infection, efficient cross-presenting cDC1 are non-infected due to their ability to
476 efficiently restrict virus replication by an IFNβ-mediated induction of cellular
477 defenses (Helft *et al*, 2012). Thus, also for *T. gondii* infection, detection of infected
478 cells by flow cytometry may not clearly distinguish the cells that have internalized
479 particulate antigens from the ones that have efficiently restricted parasite
480 replication. Activation of the IRE1α branch was observed specifically in splenic cDC1s
481 not cDC2s upon *T. gondii* infection. This result may correlate with the predominant
482 expression of TLR11/12 in cDC1 over cDC2 (Dalod *et al*, 2014; Heng *et al,* 2008) and
483 extends earlier findings in steady state showing preferential activation of the IRE1
484 branch in cDC1s (Osorio et al., 2014, Tavernier et al., 2017).
485

486 Activation of the IRE1α pathway upon *T. gondii* infection regulates key DC functions
487 required for optimal host defense (Figure 7A and 7B). Induction of XBP1s promoted
488 pro-inflammatory cytokine production at the mRNA level in a cytokine specific
489 manner. IL-6 and IL-12p40 appeared XBP1 dependent, while IL-23p19 was not. These
490 data are in line with earlier reports revealing that macrophage stimulation by TLR2
491 and TLR4 agonists activates the IRE1α pathway via a TRAF6-NOX2 axis (Martinon *et*
492 *al*, 2010). IRE1α-mediated activation of XBP1s promoted sustained production of
493 inflammatory mediators and XBP1 deficiency resulted in an increased bacterial
494 burden in mice infected with the TLR2-activating intracellular pathogen *Francisella*
495 *tularensis* (Martinon *et al*, 2010). In our hands, absence of MyD88 led to a complete
496 abrogation of *T. gondii* induced XBP1 activation. Still, it remains possible that on top
497 alternative sensing mechanisms are involved. Along these lines, a recent study
498 demonstrated that *T. gondii* infection activates IRE1α through calcium release from
499 the ER. As described previously (Urra *et al*, 2018), IRE1α oligomerization and
500 recruitment of filamin A promoted migration of *T. gondii* infected MEF and BMDCs
501 (Augusto *et al*, 2020). While this study did not investigate activation of additional
502 UPR branches in *T. gondii* infected BMDCs, these findings are consistent with our
503 results showing a sustained activation of IRE1α in infected cells (Augusto *et al*,
504 2020).
505 Besides stimulating pro-inflammatory cytokine production, we found that IRE1α, but
506 not XBP1s, was required for optimal MHCI antigen presentation of secreted *T. gondi*
507 antigens to CD8 T cells. We previously demonstrated that IRE1α–mediated RIDD
508 activity reduces MHCI antigen presentation of dead cell derived antigens by
509 degrading key factors of the cross-presentation machinery (Osorio et al. 2014). In
510 contrast to these results, upon infection, we found a role for IRE1α in promoting
511 MHCI antigen presentation. The mechanisms involved are not yet identified.
512 However, it is possible that IRE1α regulates trafficking events impacting on vacuole
513 fate, parasite antigen escape to the cytosol or on antigen processing. IRE1α
514 induction may thereby facilitate parasite control by stimulating CD8 T cell priming, a
515 process that favors preservation of the host and transmission of the parasites after
516 establishment of a chronic infection. Consistent with this hypothesis, we found that

517 mice lacking XBP1 and IRE1α failed to control the infection and succumbed during
518 the acute phase. This high susceptibility was correlated with a defect in CD4 and CD8
519 T cell expansion as well as altered CD8 T cell activation in the spleen of infected
520 mice. In line with the altered CD8 T cell proliferation and activation, IRE1α/XBP1-
521 deficient cells exhibit an altered expansion of cDC1 but not cDC2 upon infection. The
522 defect in CD4 T cell proliferation likely results from a role of cDC1 in assisting $CD8^+$ T
523 cell responses through distinct mechanisms, including a process whereby $CD4^+$ T
524 cells 'license' cDC1 for $CD8^+$ T cell priming via CD40 signaling (Smith C *et al,* 2004).
525 While our study revealed that the IRE1α pathway is essential to protect mice against
526 an acute *T. gondii* infection, it is only a first step towards understanding the likely
527 very complex process of IRE1α-mediated regulation of innate and adaptive immunity
528 against *T. gondii*. Future studies will aim to further characterize the mechanisms by
529 which activation of IRE1α and XBP1s regulates cDC1 functions upon infection,
530 including cell expansion, cytokine production and MHCI antigen presentation. It will
531 be important to also explore the role of the IRE1α branch in regulating non-lymphoid
532 tissue cDC responses, notably peripheral migratory $CD103^+$-cDC1 after oral ingestion
533 of cysts. For instance, XBP1s-mediated regulation of IL-12 production may be
534 important at early stages of parasite invasion in the intestine to activate IFNγ
535 secretion by NK cells. Thus, our study opens perspectives for the identification of
536 novel strategies to boost immunity against *T. gondii*, notably CD8 T cell responses, by
537 manipulating the UPR and thereby improve control of parasite spreading to the brain
538 and establishment of cerebral chronic infection.
539
540 **Methods**
541
542 **Mice**
543 Wild-type C57BL/6J (B6) mice were purchased from Janvier (France). C57BL/6
544 $XBP1^{fl/fl}$ (Lee *et al*, 2008), C57BL/6 XBP1ΔDC (Osorio *et al*, 2014), C57BL/6 $XBP1^{fl/fl}$
545 $IRE1^{fl/fl}$ (Iwawaki *et al*, 2010) , C57BL/6 XBP1ΔDC $IRE1^{trunc}$DC (Tavernier *et al*, 2017)
546 and ERAI mice (Iwawaki *et al*, 2004) were provided by S. Janssens (IRC/VIB, Ghent
547 University). C57BL/6 $XBP1^{fl/fl}$ $IRE1^{fl/fl}$ and C57BL/6 XBP1ΔDC $IRE1^{trunc}$DC mice were

548 bred at the « Institut Pasteur de Lille » in pathogen-free conditions. Experiments
549 were carried out in accordance with the European regulations (86/609/EEC). All
550 animal procedures were approved by the local Ethical Committee for Animal
551 Experimentation registered by the « Comité National de Réflexion Éthique
552 sur l'Expérimentation Animale » (CEEA-75). All mice were housed and bred at the
553 « Institut Pasteur de Lille » according to the protocole (APAFIS#12804-
554 2017122111233479v2) approved by the French Minister of Higher Education,
555 Research and Innovation.
556
557 **BMDC differentiation and parasite culture**
558 Wild type C57BL/6, C57BL/6 XBP1$^{fl/fl}$, C57BL/6 XBP1ΔDC, C57BL/6 XBP1$^{fl/fl}$ IRE1$^{fl/fl}$,
559 C57BL/6 XBP1ΔDC IRE1^{trunc}DC and C57BL/6 MyD88$^{-/-}$ (B. Lambrecht, IRC/VIB, Ghent
560 University) mice from 8 to 10 weeks of age were used to obtain bone marrow
561 dendritic cells (BMDCs) from the femur and tibia. BM cells were differentiated for 10
562 days in Petri dish with RPMI (Gibco™ by LifeTechnologies) supplemented with 10%
563 fetal bovin serum (FBS, Gibco™ by LifeTechnologies), 1% penicillin-streptomycin
564 (Gibco™ by LifeTechnologies), 1% sodium pyruvate (Gibco™ by LifeTechnologies),
565 0,2% 2-mercaptoethanol (Gibco™ by LifeTechnologies) and 10% Granulocyte
566 Macrophage-Colony Stimulating Factor. Flt3/Notch-differentiated DC were
567 generated as described in (Kirkling et al., 2018). Flt3 ligand was generated by the
568 protein core facility of VIB Center for Inflammation Research (Ghent, Belgium).
569
570 Tachyzoites of *Toxoplasma gondii* Type I RH Luc GFP (J.Boothroyd; Stanford
571 University of School Medicine), Type II Pru Luc GFP (J.Boothroyd; Stanford University
572 of School Medicine) and Type II Pru Tomato SAG1-Ova (Schaeffer *et al*, 2009)
573 parasites were grown *in vitro* on confluent Human Foreskin Fibroblast (HFF) cells
574 (CCD-1112Sk (ATCC, CRL-2429^{TM})) using Dulbeccos's modified Eagles medium
575 (Gibco™ by LifeTechnologies) supplemented with 10% fetal calf serum (Gibco™ by
576 LifeTechnologies), and 1% penicillin-streptomycin (Gibco™ by LifeTechnologies).
577 Prior to experiments, parasites were extracted from host cells by sequential
578 passages through 17-gauge and 26-gauge needles followed by filtration with a 3-µm
579 polycarbonate membrane filter. Parasite cultures were regularly tested for

580 mycoplasma using MycoAlert™ mycoplasma detection kit (Lonza). If not indicated
581 otherwise, BMDCs were infected at a multiplicity of infection (MOI) of 4 parasites /
582 BMDC. Heat-Killed (HK) parasites were obtained after incubation of live parasites for
583 20min at 56°C. Soluble *T. gondii* Antigens (STAgs) were obtained after lysis of
584 purified parasites by sonication in ice-cold sterile water followed by centrifugation at
585 1400rpm 30min to remove cell debris. The solution was then adjusted to 1X PBS and
586 filtered. Protein concentration was determined using the BCA kit. BMDCs were
587 incubated for 16h with STAgs at a final concentration of 10µg/mL, with tunicamycin
588 (TN) (SIGMA-ALDRICH®) at a final concentration of 1 µg/mL for 16h, with
589 lipopolysaccharide (LPS) (InvivoGen) at a final concentration of 100 ng/mL for 16h
590 and with the IRE1 inhibitor, 4µ8C (SIGMA-ALDRICH®) (Cross *et al*, 2012) at a final
591 concentration of 10µM for 16h. For *in vivo* infection, 500 parasites were injected
592 intra-peritoneally.
593
594 **Immunofluorescence assays (IFA)**
595 Adherent BMDCs on glass coverslips pre-coated with poly-L-lysine were infected
596 with parasites at a MOI of 1 during 16h before fixation with 1% paraformaldehyde
597 for 20min. After quenching with 50mM NH_4Cl for 15min, the cells were
598 permeabilized with 0,1% triton for 3min and incubated with mouse anti-KDEL (10C3
599 Enzo® Life Sciences) antibodies in 0,1% BSA-PBS, followed by DAPI and goat anti-
600 mouse secondary antibodies conjugated to Alexa Fluor 594. Images were acquired
601 using a Zeiss LSM880 confocal microscope.
602
603 **Electron microscopy**
604 BMDCs infected with *T. gondii* parasites at the MOI of 2 were fixed in 4%
605 paraformaldehyde and 2.5% glutaraldehyde in 0.1 M NaCacodylate buffer, pH 7.2
606 and centrifuged at 1500 rpm. Low melting point-agarose was used to keep the cells
607 concentrated for further processing. Cells were fixed for 4 hours at room
608 temperature followed by fixation O/N at 4°C after replacing with fresh fixative. After
609 washing in buffer, they were post-fixed in 1% OsO4 with 1.5% K3Fe(CN)6 in 0.1 M
610 NaCacodylate buffer at room temperature for 1 hour. After washing in ddH2O, cells
611 were subsequently dehydrated through a graded ethanol series, including a bulk

612 staining with 1% uranyl acetate at the 50% ethanol step followed by embedding in
613 Spurr's resin. Ultrathin sections of a gold interference color were cut using an ultra-
614 microtome (Leica EM UC7), followed by a post-staining in a Leica EM AC20 for 40
615 min in uranyl acetate at 20 °C and for 10 min in lead stain at 20°C. Sections were
616 collected on Formvar-coated copper slot grids. Grids were viewed with a JEM
617 1400plus transmission electron microscope (JEOL, Tokyo, Japan) operating at 80 kV.
618
619 **Flow cytometry**
620 After FcBlock (BD Pharmingen™) incubation, cell suspensions were labeled with a
621 dead cell marker (Aqua Live Dead Molecular Probes® by life technologies™), anti-
622 CD11c APC (N418, BioLegend®), anti-I-A/I-E (MHCII) FITC (M5/114.15.2, BioLegend®)
623 or anti-CD80 FITC (16-10A1, BioLegend®) or anti-CD86 FITC (GL-1, BioLegend®) or
624 anti-H2K^{b} FITC (AF6-88.5.5.3, BioLegend®) in PBS. After cells fixation (Fixation buffer
625 BioLegend®), samples were analyzed using the Attune NxT™ flow cytometer
626 (ThermoFisher SCIENTIFIC) and analyzed using the FlowJo10 software.
627
628 **Isolation of splenocytes**
629 Spleens were isolated from mice and digested with PBS-2% FBS containing 1mg/mL
630 of collagenase (SIGMA-ALDRICH®) and 2µg/mL of DNase I (Roche) for 20min at 37°C
631 followed by lysis of red blood cells (Red Blood Cell Lysing Buffer Hybri-Max™,
632 SIGMA-ALDRICH®). The cells were then used to perform RTqPCR, cell labeling for
633 flow cytometry or cell sorting.
634
635 **Splenic DC and T cell analysis**
636 After isolation, splenocytes were incubated with FcBlock (BD Pharmingen™). For DC
637 analysis, splenocytes were labeled with a dead cell marker (Zombie Violet™ Fixable
638 Viability, BioLegend®), anti-CD45 APC-Cy7 (30-F11, BioLegend®), anti-CD3 PE-Cy7
639 (17A2, BioLegend®), anti-CD11c APC (N418, BioLegend®), anti-I-A/I-E FITC
640 (M5/114.15.2, BioLegend®) and anti-CD8α BV605 (53-6.7, BioLegend®) antibodies in
641 PBS. CD8α-/+ DCs were isolated by cell sorting using the BD FACSARIA™ III with
642 gating on forward scatter and side scatter/singlets/live cells/CD45+ CD3- CD11c+
643 MHCII^{hi} and CD8α+ or CD8α-. For splenic T cell analysis, splenocytes were labeled

644 with a dead cell marker (Zombie Violet™ Fixable Viability, BioLegend®), anti-CD45
645 APC-Cy7 (30-F11, BioLegend®), anti-CD3 PE-Cy7 (17A2, BioLegend®), anti-CD4 AF700
646 (GK1.5, BioLegend®) and anti-CD8 BV605 (53-6.7, BioLegend®) antibodies. The
647 intracellular labeling of IFN-γ was performed according to the manufacturer's
648 instructions using anti-IFN-γ PE antibodies (XMG1.2, BioLegend®). Samples were
649 analyzed using the Attune NxT™ flow cytometer (ThermoFisher SCIENTIFIC) and the
650 FlowJo10 software.
651
652 **Quantitative real time PCR (RT-qPCR)**
653 Non-infected or infected BMDCs RNA was obtained using the RNeasy® Mini kit
654 (QIAGEN) and treated with DNase I (SIGMA-ALDRICH®). When specified, infected or
655 bystander BMDCs from a mixed population were isolated by cell sorting with gating
656 on forward scatter and side scatter/singlets/live cells/CD11c+ MHCII+/±Pru Tomato
657 Ova using the BD FACSARIA™ III. Total cDNA was generated using the High-Capacity
658 cDNA Reverse Transcription kit (Applied Biosystems™ by life technologies) according
659 to manufacturer's instructions. RT-qPCR was carried out on a QuantStudio 12K Flex
660 Real-Time PCR system (Applied Biosystems™ by life technologies) with SYBR®
661 Selected Master Mix (Life technologies) and primers (listed in Fig S5). The expression
662 of individual genes was normalized to the housekeeping gene GAPDH.
663 The RNA of CD8α+ DCs was isolated using the RNeasy® Micro kit (QIAGEN) and
664 treated with a DNase I. cDNA was generated using the SuperScript kit™ VILO™ cDNA
665 Synthesis kit (Invitrogen by Thermo Fischer Scientific) and qPCR were performed as
666 previously described.
667
668 **Western blot**
669 Non-infected or infected BMDCs were incubated with lysis buffer (250mM NaCl,
670 20mM Hepes, 1mM EDTA, 1% NP-40, 20mM DTT, phosphatase inhibitor (PhosSTOP™
671 Roche) and protease inhibitor (PROTEOLOC™)). After centrifugation, supernatants
672 were complemented with Laemmli 5X and total proteins of 2.10^5 cells were
673 subjected to electrophoresis in a 6 or 10% polyacrylamide gel. The proteins were
674 transferred onto a nitrocellulose membrane (Amersham™Protran™ 0.45µ NC) by a
675 standard western blot procedure. The membrane was blocked with 5% BSA in TBT-T

676 buffer (20mM Tris à pH 7.5, 150mM NaCl and 0.1% Tween 20) and probed with
677 primary antibodies over-night at 4°C with the following antibodies IRE1α (14C10, Cell
678 Signaling TECHNOLOGY®), XBP1s (83418, Cell Signaling TECHNOLOGY®), PERK
679 (C33E10, Cell Signaling TECHNOLOGY®), p-eIF2α (Cell Signaling TECHNOLOGY®), CHOP
680 (B-3, Santa Cruz®), GAPDH (D16H11, Cell Signaling TECHNOLOGY®) and β-tubulin (Cell
681 signaling TECHNOLOGY). Primary antibody incubation was followed by washing using
682 the TBS-T buffer prior to species specific secondary antibodies conjugated to HRP.
683 The membranes were visualized using ECL Western blotting substrate (Pierce) or
684 SuperSignal™ West Femto Maximum Sensitivity Substrate (Thermo Scientific™) on a
685 ChemiDoc™ XRS+ (BIO-RAD).
686
687 **ELISA**
688 ELISA experiments were conducted on non-infected or infected BMDCs according to
689 the manufacter's instructions using the IL-6 Mouse Uncoated ELISA kit (Invitrogen by
690 Thermo Fischer Scientific), IL-12/IL-23p40 (Total) Mouse Uncoated ELISA kit
691 (Invitrogen by Thermo Fischer Scientific) and Mouse IL-23 DuoSet® ELISA (R&D
692 SYSTEMS®). Plates were analyzed on a Spark® 10M (TECAN).
693
694 **Antigen presentation assays**
695 BMDCs were plated into flat-bottom 96-well and infected with serial dilution of
696 tachyzoïtes. The rate of infected cells (Pru Tomato SAG1-Ova detection) was
697 determined by flow cytometry. After 6h of infection, B3Z (Hosken & Bevan, 1990;
698 Karttunen *et al*, 1992) reporter hybridomas were added. After 16h of incubation
699 with B3Z, presentation of SIINFEKL (SKL8) peptide by H-2K^b was assessed by
700 quantification of β-galactosidase using the chromogenic substrate chlorophenol red-
701 β-D-galactopyranoside (CPRG, Roche). Absorbance was read at 595nm with a
702 reference at 655nm with a Spark® 10M (TECAN).
703
704 **ERAI experiment**
705 WT and ERAI mice were infected with 1000 parasites by intra-peritoneal injection.
706 Splenocytes were isolated 6 days post-infection and labeled with Live/Dead eF506
707 (eBioscience™), anti-CD45 BV605 (30-F11, BD biosciences), anti-Ly6C PerCP-eF710

708 (HK1.4, eBioscience™), anti-CD11b BUV395 (M1/70, BD biosciences), anti-CD64
709 BV711 (X54-5/7.1, BioLegend®), anti-MHCII APC-eF780 (M5/114.15.2, eBioscience™),
710 anti-CD3e PE-Cy5 (145-2C11, eBioscience™), anti-CD19 PE-Cy5 (eBio1D3(1D3),
711 eBioscience™), anti-CD11c eF450 (N418, eBioscience™), anti-CD26 APC, anti-XCR1
712 BV650 (ZET, BioLegend®) and anti-CD172a PE-Cy7 (P84, BioLegend®). The cells were
713 gated on: Non debris/Singlets/Live/CD45+/Gated out the monocytes (Ly6C^{hi}
714 CD11b++) and neutrophils (Ly6C^{INT+} CD11b+)/Gated out macrophages (CD64+ MHC-
715 II+)/Gated out T cells (CD3eCD19+ MHCII-) and B cells (CD3eCD19+ MHCII+) / CD26+
716 CD11c+ MHCII+ XCR1+ CD172a- for cDC1s and CD26+ CD11c+ MHCII+ XCR1-
717 CD172a+ for cDC2s.
718
719 **Parasite quantification by qPCR**
720 DNA extractions from splenocytes or PEC were performed with the NucleoSpin
721 Tissue kit (MACHEREY NAGEL). Individuals qPCR reactions were processed using
722 TOX9 (5'-AGGAGAGATATCAGGACTGTAG-3') and TOX11 (5'-
723 GCGTCGTCTCGTCTAGATCG-3') primers (Reischl *et al*, 2003) with SYBR® Selected
724 Master Mix (Life technologies). qPCR reactions were carried out on a QuantStudio
725 12K Flex Real-Time PCR system (Applied Biosystems™ by life technologies). Total
726 parasite number was estimated by using the average Cq for each reaction by
727 comparison to a standard curve generated with defined numbers of parasites.
728
729 **Statistical analysis**
730 All data were analyzed with Graph Pad Prism 7.0 software (San Diego, California
731 USA). Statistical analyzes are performed with the unpaired Student's t-test (with
732 Welch's correction when variances differ significantly), the Tukey's ANOVA one-way
733 test, the Tukey's ANOVA two-way test and the Log-rank test.
734
735 **Acknowledgments**
736 We thank Dr Gnangnon, Dr Fréville, Dr Lesage, Dr N'Guessan, Caroline De Witte and
737 Sophia Lafitte for help in experimental procedures. We also thank the animal facility
738 at Institut Pasteur de Lille and the BICeL flow cytometry core facility, especially Dr H.

739 Bauderlique, for technical assistance. We also thank the lab of S. Ghosh (Columbia
740 University, USA), in particular AM Shearer, C. Bussey and S. Krishnareddy.
741 SM has been supported by the Laboratoire d'Excellence (LabEx) ParaFrap from the
742 National Agency for Research ANR-11-LABX-0024 grant and a joint Chaire
743 d'Excellence from Université of Lille and the Centre National pour la Recherche
744 Scientifique (CNRS). SJ is a recipient of an ERC Consolidator Grant (Grant Number
745 819314), several FWO program grants and an EOS grant (G0G7318N). VB is holder of
746 an FWO PhD Fellowship and SR received a PhD BOF grant from the University of
747 Ghent.
748

749 **Author contributions**

750 AFP, VB, EH, SC, SR, LH, SMa, VP performed experiments. AFP, VB, EH, NB, SJ and SM
751 conceived and designed the experiments and performed data analysis. NB and JK,
752 contributed reagents, materials, and analysis tools. AFP, VB, NB, SJ and SM wrote the
753 manuscript.
754

755 **Conflict of interests**

756 The authors declare that they have no conflict of interest.
757

758 **References**

759

760 Andrade WA, Souza M do C, Ramos-Martinez E, Nagpal K, Dutra MS, Melo MB,
761 Bartholomeu DC, Ghosh S, Golenbock DT & Gazzinelli RT (2013) Combined
762 action of nucleic acid-sensing Toll-like receptors and TLR11/TLR12
763 heterodimers imparts resistance to Toxoplasma gondii in mice. *Cell Host*
764 *Microbe* 13: 42–53

765 Augusto L, Martynowicz J, Amin PH, Alakhras NS, Kaplan MH, Wek RC & Sullivan
766 WJ(2020) Toxoplasma gondii Co-opts the Unfolded Protein Response To
767 Enhance Migration and Dissemination of Infected Host Cells. *mBio* 11

768 Blanchard N, Dunay IR & Schlüter D (2015) Persistence of Toxoplasma gondii in the
769 central nervous system: a fine-tuned balance between the parasite, the brain
770 and the immune system. *Parasite Immunol* 37: 150–158

771 Bright MD, Itzhak DN, Wardell CP, Morgan GJ & Davies FE (2015) Cleavage of
772 BLOC1S1 mRNA by IRE1 Is Sequence Specific, Temporally Separate from XBP1

773 Splicing, and Dispensable for Cell Viability under Acute Endoplasmic
774 Reticulum Stress. *Mol Cell Biol* 35: 2186–2202

775 Cebrian I, Visentin G, Blanchard N, Jouve M, Bobard A, Moita C, Enninga J, Moita LF,
776 Amigorena S & Savina A (2011) Sec22b regulates phagosomal maturation and
777 antigen crosspresentation by dendritic cells. *Cell* 147: 1355–1368

778 Celli J & Tsolis RM (2015) Bacteria, the endoplasmic reticulum and the unfolded
779 protein response: friends or foes? *Nat Rev Microbiol* 13: 71–82

780 Clavarino G, Cláudio N, Dalet A, Terawaki S, Couderc T, Chasson L, Ceppi M, Schmidt
781 EK, Wenger T, Lecuit M, *et al* (2012) Protein phosphatase 1 subunit
782 Ppp1r15a/GADD34 regulates cytokine production in polyinosinic:polycytidylic
783 acid-stimulated dendritic cells. *Proc Natl Acad Sci U S A* 109: 3006–3011

784 Cubillos-Ruiz JR, Silberman PC, Rutkowski MR, Chopra S, Perales-Puchalt A, Song M,
785 Zhang S, Bettigole SE, Gupta D, Holcomb K, *et al* (2015) ER Stress Sensor XBP1
786 Controls Anti-tumor Immunity by Disrupting Dendritic Cell Homeostasis. *Cell*
787 161: 1527–1538

788 Dalet A, Argüello RJ, Combes A, Spinelli L, Jaeger S, Fallet M, Vu Manh T-P, Mendes
789 A, Perego J, Reverendo M, *et al* (2017) Protein synthesis inhibition and
790 GADD34 control IFN-β heterogeneous expression in response to dsRNA.
791 *EMBO J* 36: 761–782

792 Dalod M, Chelbi R, Malissen B & Lawrence T (2014) Dendritic cell maturation:
793 functional specialization through signaling specificity and transcriptional
794 programming. *EMBO J* 33: 1104–1116

795 Deffieu MS, Alayi TD, Slomianny C & Tomavo S (2019) The Toxoplasma gondii dense
796 granule protein TgGRA3 interacts with host Golgi and dysregulates
797 anterograde transport. *Biol Open* 8

798 Deguine J & Barton GM (2014) MyD88: a central player in innate immune signaling.
799 *F1000prime Rep* 6: 97

800 Fisch D, Clough B, Domart M-C, Encheva V, Bando H, Snijders AP, Collinson LM,
801 Yamamoto M, Shenoy AR & Frickel E-M (2020) Human GBP1 Differentially
802 Targets Salmonella and Toxoplasma to License Recognition of Microbial
803 Ligands and Caspase-Mediated Death. *Cell Rep* 32: 108008

804 Franco M, Panas MW, Marino ND, Lee M-CW, Buchholz KR, Kelly FD, Bednarski JJ,
805 Sleckman BP, Pourmand N & Boothroyd JC (2016) A Novel Secreted Protein,
806 MYR1, Is Central to Toxoplasma's Manipulation of Host Cells. *mBio* 7:
807 e02231-02215

808 Galluzzi L, Diotallevi A & Magnani M (2017) Endoplasmic reticulum stress and
809 unfolded protein response in infection by intracellular parasites. *Future Sci*
810 *OA* 3: FSO198

811 Goldszmid RS, Coppens I, Lev A, Caspar P, Mellman I & Sher A (2009) Host ER-
812 parasitophorous vacuole interaction provides a route of entry for antigen
813 cross-presentation in Toxoplasma gondii-infected dendritic cells. *J Exp Med*
814 206: 399–410

815 Grootjans J, Kaser A, Kaufman RJ & Blumberg RS (2016) The unfolded protein
816 response in immunity and inflammation. *Nat Rev Immunol* 16: 469–484

817 Gubbels M-J, Striepen B, Shastri N, Turkoz M & Robey EA (2005) Class I major
818 histocompatibility complex presentation of antigens that escape from the
819 parasitophorous vacuole of Toxoplasma gondii. *Infect Immun* 73: 703–711

820 Hakimi M-A, Olias P & Sibley LD (2017) Toxoplasma Effectors Targeting Host
821 Signaling and Transcription. *Clin Microbiol Rev* 30: 615–645

822 Helft J, Manicassamy B, Guermonprez P, Hashimoto D, Silvin A, Agudo J, Brown BD,
823 Schmolke M, Miller JC, Leboeuf M, *et al* (2012) Cross-presenting CD103+
824 dendritic cells are protected from influenza virus infection. *J Clin Invest* 122:
825 4037–4047

826 Heng TSP, Painter MW & Immunological Genome Project Consortium (2008) The
827 Immunological Genome Project: networks of gene expression in immune
828 cells. *Nat Immunol* 9: 1091–1094

829 Hollien J, Lin JH, Li H, Stevens N, Walter P & Weissman JS (2009) Regulated Ire1-
830 dependent decay of messenger RNAs in mammalian cells. *J Cell Biol* 186:
831 323–331

832 Hou B, Benson A, Kuzmich L, DeFranco AL & Yarovinsky F (2011) Critical coordination
833 of innate immune defense against Toxoplasma gondii by dendritic cells
834 responding via their Toll-like receptors. *Proc Natl Acad Sci U S A* 108: 278–283

835 Iwawaki T, Kohno K & Miura M (2004) Transgenic mouse model for monitoring
836 endoplasmic reticulum stress in vivo. *Nat Med* 10: 1014–1014

837 John B, Harris TH, Tait ED, Wilson EH, Gregg B, Ng LG, Mrass P, Roos DS, Dzierszinski
838 F, Weninger W, *et al* (2009) Dynamic Imaging of CD8(+) T cells and dendritic
839 cells during infection with Toxoplasma gondii. *PLoS Pathog* 5: e1000505

840 Kim JY, Ahn H-J, Ryu KJ & Nam H-W (2008) Interaction between parasitophorous
841 vacuolar membrane-associated GRA3 and calcium modulating ligand of host
842 cell endoplasmic reticulum in the parasitism of Toxoplasma gondii. *Korean J*
843 *Parasitol* 46: 209–216

844 Kirkling ME, Cytlak U, Lau CM, Lewis KL, Resteu A, Khodadadi-Jamayran A, Siebel CW,
845 Salmon H, Merad M, Tsirigos A, *et al* (2018) Notch Signaling Facilitates
846 In Vitro Generation of Cross-Presenting Classical Dendritic Cells. *Cell Rep* 23:
847 3658-3672.e6

848 Koblansky AA, Jankovic D, Oh H, Hieny S, Sungnak W, Mathur R, Hayden MS, Akira S,
849 Sher A & Ghosh S (2013) Recognition of profilin by Toll-like receptor 12 is
850 critical for host resistance to Toxoplasma gondii. *Immunity* 38: 119–130

851 Kongsomboonvech AK, Rodriguez F, Diep AL, Justice BM, Castallanos BE, Camejo A,
852 Mukhopadhyay D, Taylor GA, Yamamoto M, Saeij JPJ, *et al* (2020) Naïve CD8
853 T cell IFNγ responses to a vacuolar antigen are regulated by an
854 inflammasome-independent NLRP3 pathway and Toxoplasma gondii ROP5.
855 *PLoS Pathog* 16: e1008327

856 Lee A-H, Scapa EF, Cohen DE & Glimcher LH (2008) Regulation of hepatic lipogenesis
857 by the transcription factor XBP1. *Science* 320: 1492–1496

858 Lee Y, Sasai M, Ma JS, Sakaguchi N, Ohshima J, Bando H, Saitoh T, Akira S &
859 Yamamoto M (2015) p62 Plays a Specific Role in Interferon-γ-Induced
860 Presentation of a Toxoplasma Vacuolar Antigen. *Cell Rep* 13: 223–233

861 Márquez S, Fernández JJ, Terán-Cabanillas E, Herrero C, Alonso S, Azogil A, Montero
862 O, Iwawaki T, Cubillos-Ruiz JR, Fernández N, *et al* (2017) Endoplasmic
863 Reticulum Stress Sensor IRE1α Enhances IL-23 Expression by Human Dendritic
864 Cells. *Front Immunol* 8: 639

865 Martinon F, Chen X, Lee A-H & Glimcher LH (2010) Toll-like receptor activation of
866 XBP1 regulates innate immune responses in macrophages. *Nat Immunol* 11:
867 411–418

868 Medel B, Costoya C, Fernandez D, Pereda C, Lladser A, Sauma D, Pacheco R, Iwawaki
869 T, Salazar-Onfray F & Osorio F (2018) IRE1α Activation in Bone Marrow-
870 Derived Dendritic Cells Modulates Innate Recognition of Melanoma Cells and
871 Favors CD8+ T Cell Priming. *Front Immunol* 9: 3050

872 Mogilenko DA, Haas JT, L'homme L, Fleury S, Quemener S, Levavasseur M, Becquart
873 C, Wartelle J, Bogomolova A, Pineau L, *et al* (2019) Metabolic and Innate
874 Immune Cues Merge into a Specific Inflammatory Response via the UPR. *Cell*
875 177: 1201-1216.e19

876 Naor A, Panas MW, Marino N, Coffey MJ, Tonkin CJ & Boothroyd JC (2018) MYR1-
877 Dependent Effectors Are the Major Drivers of a Host Cell's Early Response to
878 Toxoplasma, Including Counteracting MYR1-Independent Effects. *mBio* 9

879 Novoa I, Zeng H, Harding HP & Ron D (2001) Feedback inhibition of the unfolded
880 protein response by GADD34-mediated dephosphorylation of eIF2alpha. *J*
881 *Cell Biol* 153: 1011–1022

882 Osorio F, Lambrecht BN & Janssens S (2018) Antigen presentation unfolded:
883 identifying convergence points between the UPR and antigen presentation
884 pathways. *Curr Opin Immunol* 52: 100–107

885 Osorio F, Tavernier SJ, Hoffmann E, Saeys Y, Martens L, Vetters J, Delrue I, De Rycke
886 R, Parthoens E, Pouliot P, *et al* (2014) The unfolded-protein-response sensor
887 IRE-1α regulates the function of CD8α+ dendritic cells. *Nat Immunol* 15: 248–
888 257

889 Panas MW, Naor A, Cygan AM & Boothroyd JC (2019) Toxoplasma Controls Host
890 Cyclin E Expression through the Use of a Novel MYR1-Dependent Effector
891 Protein, HCE1. *mBio* 10

892 Pernas L, Adomako-Ankomah Y, Shastri AJ, Ewald SE, Treeck M, Boyle JP &
893 Boothroyd JC (2014) Toxoplasma effector MAF1 mediates recruitment of host
894 mitochondria and impacts the host response. *PLoS Biol* 12: e1001845

895 Pernas L, Bean C, Boothroyd JC & Scorrano L (2018) Mitochondria Restrict Growth of
896 the Intracellular Parasite Toxoplasma gondii by Limiting Its Uptake of Fatty
897 Acids. *Cell Metab* 27: 886-897.e4

898 Poncet AF, Blanchard N & Marion S (2019) Toxoplasma and Dendritic Cells: An
899 Intimate Relationship That Deserves Further Scrutiny. *Trends Parasitol* 35:
900 870–886

901 Rathore APS, Ng M-L & Vasudevan SG (2013) Differential unfolded protein response
902 during Chikungunya and Sindbis virus infection: CHIKV nsP4 suppresses eIF2α
903 phosphorylation. *Virol J* 10: 36

904 Reverendo M, Mendes A, Argüello RJ, Gatti E & Pierre P (2019) At the crossway of
905 ER-stress and proinflammatory responses. *FEBS J* 286: 297–310

906 Romano JD, Nolan SJ, Porter C, Ehrenman K, Hartman EJ, Hsia R-C & Coppens I (2017)
907 The parasite Toxoplasma sequesters diverse Rab host vesicles within an
908 intravacuolar network. *J Cell Biol* 216: 4235–4254

909 Sardinha-Silva A, Mendonça-Natividade FC, Pinzan CF, Lopes CD, Costa DL, Jacot D,
910 Fernandes FF, Zorzetto-Fernandes ALV, Gay NJ, Sher A, *et al* (2019) The
911 lectin-specific activity of Toxoplasma gondii microneme proteins 1 and 4
912 binds Toll-like receptor 2 and 4 N-glycans to regulate innate immune priming.
913 *PLoS Pathog* 15: e1007871

914 Shoulders MD, Ryno LM, Genereux JC, Moresco JJ, Tu PG, Wu C, Yates JR, Su AI, Kelly
915 JW & Wiseman RL (2013) Stress-independent activation of XBP1s and/or
916 ATF6 reveals three functionally diverse ER proteostasis environments. *Cell*
917 *Rep* 3: 1279–1292

918 Sinai AP, Webster P & Joiner KA (1997) Association of host cell endoplasmic
919 reticulum and mitochondria with the Toxoplasma gondii parasitophorous
920 vacuole membrane: a high affinity interaction. *J Cell Sci* 110 (Pt 17): 2117–
921 2128

922 Smith CM, Wilson NS, Waithman J, Villadangos JA, Carbone FR, Heath WR & Belz GT
923 (2004) Cognate CD4(+) T cell licensing of dendritic cells in CD8(+) T cell
924 immunity. *Nat Immunol* 5: 1143–1148

925 Smith JA (2018) Regulation of Cytokine Production by the Unfolded Protein
926 Response; Implications for Infection and Autoimmunity. *Front Immunol* 9:
927 422

928 Sriburi R, Bommiasamy H, Buldak GL, Robbins GR, Frank M, Jackowski S & Brewer JW
929 (2007) Coordinate regulation of phospholipid biosynthesis and secretory
930 pathway gene expression in XBP-1(S)-induced endoplasmic reticulum
931 biogenesis. *J Biol Chem* 282: 7024–7034

932 Tavernier SJ, Osorio F, Vandersarren L, Vetters J, Vanlangenakker N, Van Isterdael G,
933 Vergote K, De Rycke R, Parthoens E, van de Laar L, *et al* (2017) Regulated
934 IRE1-dependent mRNA decay sets the threshold for dendritic cell survival.
935 *Nat Cell Biol* 19: 698–710

936 Urra H, Henriquez DR, Cánovas J, Villarroel-Campos D, Carreras-Sureda A, Pulgar E,
937 Molina E, Hazari YM, Limia CM, Alvarez-Rojas S, *et al* (2018) IRE1α governs
938 cytoskeleton remodelling and cell migration through a direct interaction with
939 filamin A. *Nat Cell Biol* 20: 942–953

940 Walter P & Ron D (2011) The unfolded protein response: from stress pathway to
941 homeostatic regulation. *Science* 334: 1081–1086

942 Woo CW, Cui D, Arellano J, Dorweiler B, Harding H, Fitzgerald KA, Ron D & Tabas I
943 (2009) Adaptive suppression of the ATF4-CHOP branch of the unfolded
944 protein response by toll-like receptor signalling. *Nat Cell Biol* 11: 1473–1480

945 Woo CW, Kutzler L, Kimball SR & Tabas I (2012) Toll-like receptor activation
946 suppresses ER stress factor CHOP and translation inhibition through
947 activation of eIF2B. *Nat Cell Biol* 14: 192–200

948 Yamamoto M, Ma JS, Mueller C, Kamiyama N, Saiga H, Kubo E, Kimura T, Okamoto T,
949 Okuyama M, Kayama H, *et al* (2011) ATF6beta is a host cellular target of the
950 Toxoplasma gondii virulence factor ROP18. *J Exp Med* 208: 1533–1546

951 Yarovinsky F, Zhang D, Andersen JF, Bannenberg GL, Serhan CN, Hayden MS, Hieny S,
952 Sutterwala FS, Flavell RA, Ghosh S, *et al* (2005) TLR11 activation of dendritic
953 cells by a protozoan profilin-like protein. *Science* 308: 1626–1629

954 Yoshida H, Matsui T, Yamamoto A, Okada T & Mori K (2001) XBP1 mRNA is induced
955 by ATF6 and spliced by IRE1 in response to ER stress to produce a highly
956 active transcription factor. *Cell* 107: 881–891

957 Zhang Y, Chen G, Liu Z, Tian S, Zhang J, Carey CD, Murphy KM, Storkus WJ, Falo LD &
958 You Z (2015) Genetic vaccines to potentiate the effective CD103+ dendritic

959 cell-mediated cross-priming of antitumor immunity. *J Immunol Baltim Md*
960 *1950* 194: 5937–5947

961
962
963 **Figure Legends**
964
965 **Figure 1. The IRE1α/ XBP1s pathway is activated in BMDCs infected with *T. gondii.***
966 BMDCs were infected with Pru parasites (at a MOI of 4 parasites/BMDC) or treated
967 with tunicamycin (TN) for 16h and the expression of UPR target genes were analyzed
968 by RT-qPCR. The results are expressed as (Log2) Fold change **(A)** or relative mRNA
969 level **(B)** compared to non-infected (NI) conditions. IRE1α/XBP1s pathway: *Ern1*
970 (IRE1α), *Xbp1s, Dnajb9* (ERdj4)*, Sec24D, Bloc1s1 and Sec61a1* **-** PERK/ATF4 pathway:
971 *Atf4, Ddit3* (CHOP) and *Ppp1r15a* (GADD34) - ATF6 pathway: *Atf6 and Herpud1*;
972 classical ER chaperons: *Hspa5* (BIP) and *Hsp90b1* (GRP94). Results are normalized to
973 the housekeeping gene *Gapdh.* Unpaired Student T-test, ns: p>0.05; **: p<0.01; ***:
974 p<0.001; mean ± S.E.M (n=3-14 mice). **(C, D)** Immunoblot analysis of IRE1α, PERK,
975 Phospho-PERK (detected by the presence of a second upper band after migration on
976 a 6% acrylamide gel), Phospho-eIF2α, CHOP and XBP1s protein expression in non-
977 infected BMDCs, BMDCs treated with TN and Pru infected BMDCs (**C**) and in non-
978 infected and Pru infected Flt3/Notch-DCs (**D**) for the indicated times. GAPDH and
979 tubulin were used as loading controls.
980
981 **Figure 2. UPR and cytokine responses are under the control of MyD88 protein in**
982 **BMDCs infected with *T. gondii*. (A)** Mean percentage of Pru parasite infection of WT
983 and MyD88KO BMDCs; mean ± S.E.M (n=3 mice). **(B)** Mean percentage of
984 parasitophorous vacuoles containing 1, 2, 4 or 8 parasites/vacuole (p/v) in WT and
985 MyD88 KO BMDCs after 16h of infection with Pru parasites. Mean values ± SEM of
986 three independent experiments are shown. **(C)** IL-6, IL-12 and IL-23 cytokine levels
987 from WT and MyD88KO BMDCs non-infected (NI) and infected with Pru parasites for
988 16h. Two-way ANOVA Tukey's multiple comparisons, ****: p<0.0001; mean ± S.E.M
989 (n=4-6 mice, 2 independent experiments combined). **(D)** mRNA relative expression
990 level of *Xbp1s, Dnajb9* (ERdj4), *Ddit3* (CHOP) and *Ppp1r15a* (GADD34) from WT and
991 MyD88KO BMDCs infected with Pru parasites for 16h compared to non-infected (NI)
992 conditions. Results are normalized to the housekeeping gene *Gapdh*. Two-way
993 ANOVA Tukey's multiple comparisons, ns: p>0.05; *: p<0.05; **: p<0.01; ***:
994 p<0.001, ****: p<0.0001; mean ± S.E.M (n=4-5 mice, 2 independent experiments
995 combined).
996
997 **Figure 3**. **Replicating parasites modulate the UPR. (A)** BMDCs were incubated with
998 Pru-Tomato parasites for 16h. Infected cells (red gating) and non-infected bystander
999 cells (green gating) were sorted-purified. **(B)** The expression of UPR target genes
1000 were analyzed by RT-qPCR in infected and non-infected bystander cells compared to
1001 non-infected BMDCs (NI). The results are expressed as relative mRNA level
1002 compared to non-infected conditions. Results are normalized to the housekeeping
1003 gene *Gapdh.* Unpaired Student T-test, ns: p>0.05; *: p<0.05; **: p<0.01; ***:
1004 p<0.001; mean ± S.E.M (n=6 mice, 2 independent experiments combined).

1005
1006
1007 **Figure 4. The IRE1α/XBP1s pathway modulates cytokine responses in infected**
1008 **BMDCs and cross-presentation of soluble secreted parasite antigens.**
1009 **(A)** Dotplots showing the percentage of CD11c^{+}/MHCII^{hi} cells in Pru Tomato SAG1-
1010 OVA parasite infected XBP1$^{fl/fl}$, XBP1ΔDC, XBP1$^{fl/fl}$IRE1$^{fl/fl}$ and XBP1ΔDC IRE1^{trunc}DC
1011 BMDCs (upper panels) and of Tomato-positive cells (percentage of infected BMDCs:
1012 lower panels). **(B)** Mean percentage ± S.E.M of infection is indicated (n=6 mice). **(C)**
1013 Mean percentage of parasitophorous vacuoles containing 1, 2, 4 or 8
1014 parasites/vacuole (p/vac) in XBP1$^{fl/fl}$IRE1$^{fl/fl}$, XBP1ΔDC IRE1^{trunc}DC and XBP1ΔDC
1015 BMDCs (n=3 independent experiments). **(D)** IL-6, IL-12 and IL-23 secreted cytokine
1016 levels from Pru parasite infected XBP1$^{fl/fl}$, XBP1ΔDC, XBP1$^{fl/fl}$IRE1$^{fl/fl}$ and XBP1ΔDC
1017 IRE1^{trunc}DC BMDCs measured by ELISA. Two-way ANOVA Tukey's multiple
1018 comparisons, ns: p>0.05; ***: p<0.001; ****: p<0.0001; mean ± S.E.M (n=5-6 mice, 2
1019 independent experiments combined). **(E)** mRNA relative expression level of *Il-6*, *Il-12*
1020 and *Il-23* from XBP1$^{fl/fl}$IRE1$^{fl/fl}$, XBP1ΔDC IRE1^{trunc}DC and XBP1ΔDC BMDCs infected
1021 with Pru parasites for 16 h compared to non-infected (NI) conditions. Results are
1022 normalized to the housekeeping gene *Gapdh*. Two-way ANOVA Tukey's multiple
1023 comparisons, ns: p>0.05; *: p<0.05; **: p<0.01; ***: p<0.001; ****: p<0.0001; mean
1024 ± S.E.M (n=3-5 mice, 2 independent experiments combined). **(F)** H-2K^{b}-SKL8 MHC
1025 class I presentation by XBP1$^{fl/fl}$IRE1$^{fl/fl}$ treated or not with 4μ8C, XBP1ΔDC IRE1^{trunc}DC
1026 and XBP1ΔDC BMDCs infected with Pru Tomato SAG1-OVA at the indicated ratios,
1027 assessed with the B3Z T cell hybridoma. Unpaired Student T-test, *: p<0.05; **:
1028 p<0.01; ***: p<0.001; mean ± S.E.M (n=3 mice, one representative experiment out
1029 of 2). **(G)** Percentage of Pru Tomato SAG1-OVA infected BMDCs at the indicated
1030 ratios of parasites:BMDC. Bar graphs depict mean ± S.E.M (n=3 mice, one
1031 representative experiment from 2 independent experiments). **(H)** Exogenous MHCI
1032 presentation of synthetic SKL8 peptide pulsed on XBP1$^{fl/fl}$IRE1$^{fl/fl}$ treated or not with
1033 4μ8C, XBP1ΔDC IRE1^{trunc}DC and XBP1ΔDC BMDCs assessed with the B3Z T cell
1034 hybridoma. Bar graphs depict mean ± S.E.M (n=3 mice, one representative
1035 experiment from 2 independent experiments). **(I)** Graph depicts the expression
1036 (indicated as the Mean Fluorescence Intensity) of H-2K^{b} by Pru Tomato SAG1-OVA
1037 infected XBP1$^{fl/fl}$ IRE1$^{fl/fl}$ treated or not with 4μ8C, XBP1ΔDC IRE1^{trunc}DC and XBP1ΔDC
1038 BMDCs. Bar graphs depict mean ± S.E.M (n=3 mice, one representative experiment
1039 from 2 independent experiments).
1040
1041 **Figure 5: The IRE1α/XBP1s pathway is activated in splenic cDC1 of mice infected**
1042 **with *T. gondii*. (A, B)** Expression of VenusFP by splenic cDC1 (CD26+ CD11c+ MHCII+
1043 XCR1+ CD172a-, upper panels) and cDC2 (CD26+ CD11c+ MHCII+ XCR1- CD172a+,
1044 lower panel) from WT **(A)** and ERAI **(B)** mice non-infected (NI) or infected with Pru (6
1045 days post-infection (dpi)) reporting on IRE1α pathway activation. **(C)** Graph depicts
1046 the Mean Fluorescence Intensity measured for each condition in ERAI mice (6 dpi).
1047 Two-way ANOVA Tukey's multiple comparisons, ns: p>0.05; ***: p<0.001; ****:
1048 p<0.0001; mean ± S.E.M (n=5 mice per genotype and condition, one representative
1049 experiment from 2 independent experiments). **(D)** Graph depicts the expression
1050 (indicated as the Mean Fluorescence Intensity) of VenusFP by splenic monocytes,
1051 neutrophils, B and T cells from Pru infected or non-infected (NI) ERAI mice (6 dpi).

1052 Bar graphs depict mean ± S.E.M (n=5 mice per genotype and condition, one
1053 representative experiment from 2 independent experiments). **(E**, **F)** RT-qPCR analysis
1054 of the indicated UPR genes among total RNA prepared from splenic cDC1 **(E)** and
1055 cDC2 **(F)** sorted by flow cytometry 6 dpi from wild-type mice, non-infected (NI) or
1056 infected with Pru parasites. Results were normalized to the housekeeping gene
1057 *Gapdh* and are expressed as relative mRNA level compared to the NI condition. Bar
1058 graphs depict mean ± S.E.M. Unpaired Student T-test, ns: p>0.05; *: p<0.05; **:
1059 p<0.01; mean ± S.E.M (n=3-5 mice).
1060
1061 **Figure 6. The IRE1α pathway protects mice from acute infection and promotes T**
1062 **cell responses. (A)** Survival curves of XBP1$^{fl/fl}$IRE1$^{fl/fl}$ and XBP1ΔDC IRE1^{trunc}DC mice
1063 infected intraperitoneally with 500 Pru parasites. Log-rank (Mantel-Cox) test,
1064 p=0,0004; n=10 mice per genotype. **(B)** Number of parasite genomes per spleen and
1065 PEC from XBP1$^{fl/fl}$IRE1$^{fl/fl}$ and XBP1ΔDC IRE1^{trunc}DC infected intraperitoneally with 500
1066 Pru parasites 6 days post-infection. Unpaired Student T-test **: p<0.01; mean ±
1067 S.E.M (n=6-7 mice per genotype, 2 independent experiments combined). **(C)** mRNA
1068 relative expression of *Il-6, Il-12, Ifn-g* and *Tnf-a* by splenocytes from XBP1$^{fl/fl}$IRE1$^{fl/fl}$
1069 and XBP1ΔDC IRE1^{trunc}DC mice infected or not (NI) with 500 Pru parasites for 6 days.
1070 Results are normalized to the housekeeping gene *Gapdh.* Two-way ANOVA Tukey's
1071 multiple comparisons, ns: p>0.05; *: p<0.05; **: p<0.01; ****: p<0.0001; mean ±
1072 S.E.M (n=5-7 mice, 2 independent experiments combined). **(D, E)** Quantification of
1073 the number of total (left histogram) and activated (right histogram) (IFNγ-positive)
1074 CD4+ T cells **(D)** and CD8+ T cells **(E)** in the spleen of control mice (XBP1$^{fl/fl}$IRE1$^{fl/fl}$)
1075 and XBP1ΔDC IRE1^{trunc}DC infected for 6 days. Two-way ANOVA Tukey's multiple
1076 compare, ns: p> 0.05; *: p <0.05; **: p <0.01; ***: p <0.001; ****: p <0.0001; mean ±
1077 S.E.M (n=5-8 mice, 2 independent experiments combined). (**F**) Frequency and
1078 number of cDC2 (left) and cDC1 (right) in the spleen of control mice and XBP1ΔDC
1079 IRE1^{trunc}DC infected for 6 days. Two-way ANOVA Tukey's multiple compare, ns: p>
1080 0.05; ****: p <0.0001; mean ± S.E.M (n=7 mice, 2 independent experiments
1081 combined).
1082
1083 **Figure 7: Modulation of the UPR and down-stream responses in *T. gondii* infected**
1084 **BMDCs.**
1085 **(A)** After incubation of BMDCs with HK parasites or STAg, TLRs are stimulated and
1086 induce transcriptional activation of the three pathways of the UPR. The IRE1α/XBP1s
1087 pathway stimulates the secretion of IL-6 and IL-12 by BMDCs.
1088 **(B)** In BMDCs infected with live Pru parasites for 16h, the IRE1α/XBP1s pathway is
1089 activated in a MyD88-dependent manner while the PERK pathway is not induced and
1090 the ATF6 pathway is repressed. XBP1s stimulates the secretion of IL-6 and IL-12 and
1091 IRE1α promotes MHC-I presentation of secreted parasite antigens. The secretion of
1092 IL-23 is independent of XBP1s and CHOP and only partially depends on MyD88. Our
1093 data also indicate that live parasites down-regulate the induction of XBP1s and CHOP
1094 induced by TLRs.
1095 Blue arrows indicate down-regulated pathways and red arrows, up-regulated
1096 pathways.
1097
1098 **Expanded View Figure Legends**

1099
1100 **Figure EV1**. **Induction of cytokine production from infected BMDCs. (A)** IL-6, IL-12
1101 and IL-23 cytokine levels from non-infected BMDCs (NI) and BMDCs infected with
1102 Pru parasites for 6h and 16h measured by ELISA. Unpaired Student T-test, *: p<0.05;
1103 **: p<0.01; ***: p<0.001; mean ± S.E.M (n=4-6 mice, 2 independent experiments
1104 combined). **(B)** IL-6, IL-12 and IL-23 cytokine levels from non-infected BMDCs (NI)
1105 and type I RH or type II Pru infected BMDCs measured by ELISA. ANOVA Tukey's
1106 multiple comparisons, ns: p>0.05; *: p<0.05; **: p<0.01; ***: p<0.001, ****:
1107 p<0.0001; mean ± S.E.M (n=4-6 mice, 2 independent experiments).
1108
1109 **Figure EV2. hER is recruited at the PV of infected BMDCs**. **(A)** Electron microscopy
1110 images showing the recruitment of hER at the limiting membrane of vacuole
1111 containing live Pru parasites. Right images (bars=500nm): zoom of the region
1112 indicated by a white frame on the left images (bars=1μm). **(B)** Pru Heat-killed (HK)
1113 parasite containing vacuoles do not recruit hER.
1114
1115
1116 **Figure EV3. The three pathways of the UPR response are activated in BMDCs**
1117 **incubated with Pru HK parasites and STAgs. (A)** BMDCs were incubated with Pru HK
1118 parasites for 16h and the expression of UPR target genes were analyzed by RT-qPCR.
1119 The results are expressed as relative mRNA level compared to non-infected
1120 conditions. Results are normalized to the housekeeping gene *Gapdh.* Unpaired
1121 Student T-test, **: p<0.01; ***: p<0.001; ****: p<0.0001; mean ± S.E.M (n=3-14
1122 mice). **(B, C)** Immunoblot analysis of IRE1α, phospho-eIF2a, CHOP and XBP1s protein
1123 expression in non-infected BMDCs, BMDCs treated with tunicamycin (TN), BMDCs
1124 incubated with Pru live parasites and BMDCs incubated with Pru HK parasites for the
1125 indicated times. GAPDH and tubulin were used as loading controls. **(D)** Immunoblot
1126 analysis of IRE1α and XBP1s in non-infected BMDCs (NI), BMDCs infected with Pru
1127 parasites for 16h and treated with soluble *T. gondii* antigen extracts (STAgs) for 16h.
1128 Tubulin was used as loading control. **(E)** BMDCs were incubated with STAgs for 16h
1129 and the expression of UPR target genes were analyzed by RT-qPCR. The results are
1130 expressed as relative mRNA level compared to non-infected conditions. Results are
1131 normalized to the housekeeping gene *gapdh.* Unpaired Student T-test, ns: p>0.05;
1132 **: p<0.01; ***: p<0.001; mean ± S.E.M (n=4 mice).
1133
1134 **Figure EV4. UPR and cytokine responses are under the control of MyD88 in BMDCs**
1135 **incubated with Heat-Killed parasites (A)** mRNA relative expression level of *Xbp1s,*
1136 *Dnajb9* (ERdj4), *Ddit3* (CHOP) and *Ppp1r15a* (GADD34) from WT and MyD88KO
1137 BMDCs incubated with Heat-Killed (HK) parasites for 16h compared to non-infected
1138 (NI) condition. Results are normalized to the housekeeping gene *Gapdh*. Two-way
1139 ANOVA Tukey's multiple comparisons, ns: p>0.05; ****: p<0.0001; mean ± S.E.M.
1140 (n=4-5 mice, 2 independent experiments combined) **(B)** IL-6, IL-12 and IL-23 cytokine
1141 levels from WT and MyD88 KO BMDCs non-infected (NI), infected with Pru parasites
1142 or incubated with Pru HK parasites for 16 h. Two-way ANOVA Tukey's multiple
1143 comparisons, ****: p<0.0001; mean ± S.E.M (n=4-6 mice, 2 independent
1144 experiments combined).
1145

1146 **Figure EV5. IRE1α/XBP1s depletion does not impact on BMDC differentiation and**
1147 **activation. (A)** Immunoblot analysis of IRE1α and XBP1s protein expression in
1148 XBP1$^{fl/fl}$IRE1$^{fl/fl}$, XBP1ΔDC and XBP1ΔDC IRE1^{trunc}DC BMDCs treated or not with
1149 tunicamycin (TN) to induce ER stress. Please note that there is never 100% excision
1150 of the floxed alleles in GM-CSF BMDCs cultures, as can be noted from the strongly
1151 reduced but not fully abrogated expression of IRE1α and truncated IRE1α remaining
1152 visible in the XBP1ΔDC IRE1^{trunc}DC BMDCs line. **(B)** Dotplots showing the percentage
1153 of live cells (live/dead marker, upper panels) and of cells expressing CD11c and
1154 MHCII molecules (lower panels) in Pru infected XBP1$^{fl/fl}$IRE1$^{fl/fl}$, XBP1ΔDC IRE1^{trunc}DC
1155 and XBP1ΔDC BMDCs. Graph depicts the mean percentage of live cells and CD11c+
1156 MHCII ^{high} cells in XBP1$^{fl/fl}$IRE1$^{fl/fl}$, XBP1ΔDC IRE1^{trunc}DC and XBP1ΔDC BMDCs non-
1157 infected (NI), infected with Pru parasites, incubated with Pru HK parasites or treated
1158 with LPS for 16h. Bar graphs depict mean ± S.E.M (n=3 mice). **(C)** Staining profiles of
1159 LPS treated XBP1$^{fl/fl}$IRE1$^{fl/fl}$, XBP1ΔDC IRE1^{trunc}DC and XBP1ΔDC BMDCs indicating the
1160 surface expression of CD80 and CD86 molecules. Graph depicts the quantification
1161 (indicated as the Mean Fluorescence Intensity) of CD80 and CD86 expression in LPS
1162 treated XBP1$^{fl/fl}$IRE1$^{fl/fl}$, XBP1ΔDC IRE1^{trunc}DC and XBP1ΔDC BMDCs. Bar graphs depict
1163 mean ± S.E.M (n=3 mice).
1164
1165 **Figure EV6. XBP1s regulates cytokine production in BMDCs incubated with heat-**
1166 **killed parasites. (A)** IL-6, IL-12 and IL-23 cytokine levels from XBP1$^{fl/fl}$, XBP1ΔDC,
1167 XBP1$^{fl/fl}$IRE1$^{fl/fl}$ and XBP1ΔDC IRE1^{trunc}DC BMDCs infected with Pru parasites or
1168 incubated with Pru Heat-Killed (HK) parasites for 16h compared to non-infected (NI)
1169 BMDCs. Two-way ANOVA Tukey's multiple comparisons test, ns: $p>0.05$; *: $p<0.05$;
1170 **: $p<0.01$; ****: $p<0.0001$; mean ± S.E.M (n=3-6 mice from 2 independent
1171 experiments). **(B)** mRNA relative expression of *Il-6, Il-12* and *Il-23* from
1172 XBP1$^{fl/fl}$IRE1$^{fl/fl}$, XBP1ΔDC IRE1^{trunc}DC and XBP1ΔDC BMDCs infected with Pru
1173 parasites or incubated with Pru Heat-Killed (HK) parasites for 16h compared to non-
1174 infected (NI) BMDCs. Results are normalized to the housekeeping gene *Gapdh.* Two-
1175 way ANOVA Tukey's multiple comparisons test, ns $p>0.05$; * $p<0.05$; ** $p<0.01$; ****
1176 $p<0.0001$; mean ± S.E.M (n=3-6 mice from 2 independent experiments).
1177
1178

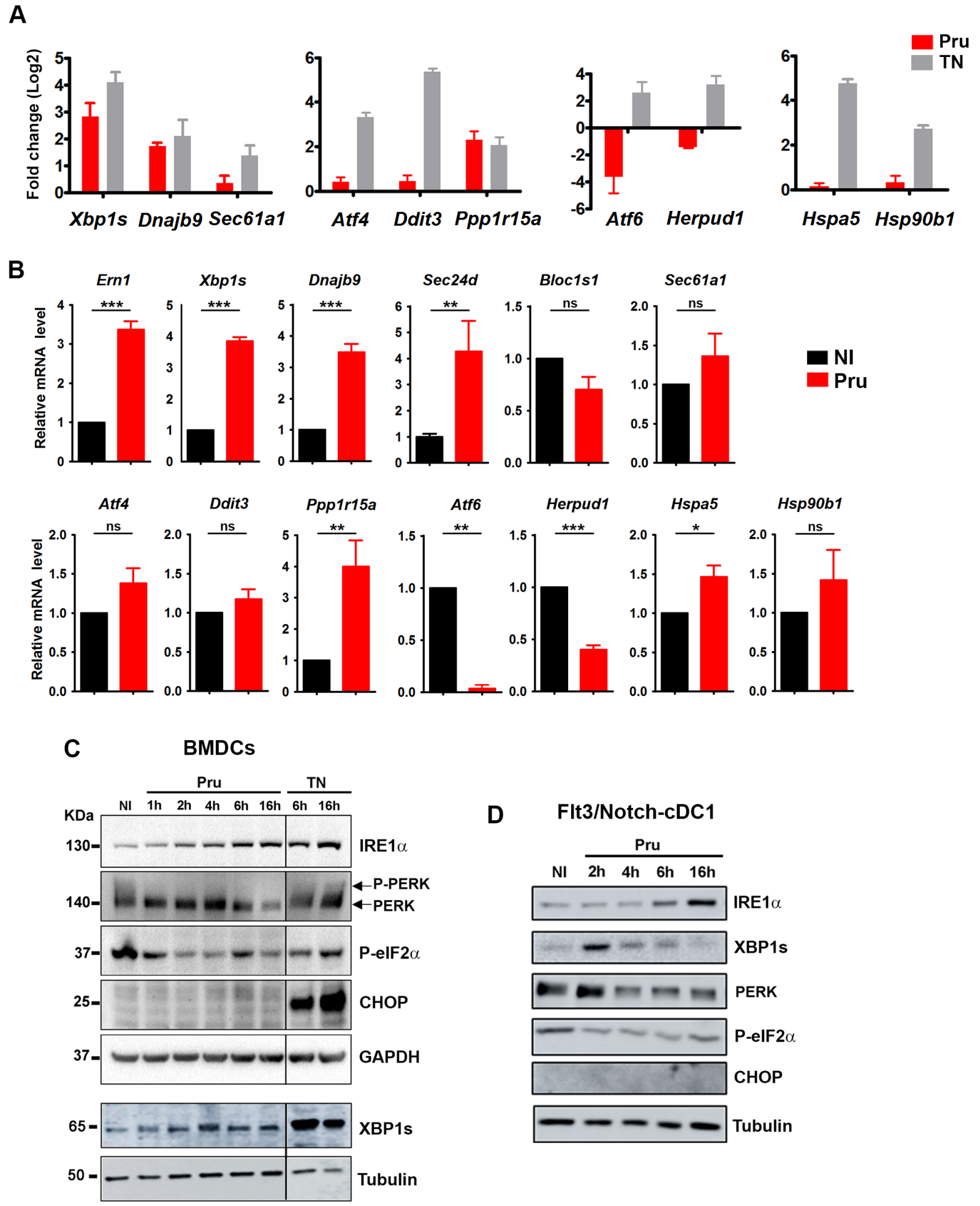
A
Fold change (Log2)
Pru
TN
Xbp1s
Dnajb9
Sec61a1
Atf4
Ddit3
Ppp1r15a
Atf6
Herpud1
Hspa5
Hsp90b1
B
Relative mRNA level
NI
Pru
Ern1
Xbp1s
Dnajb9
Sec24d
Bloc1s1
Sec61a1
Atf4
Ddit3
Ppp1r15a
Atf6
Herpud1
Hspa5
Hsp90b1
***
**
*
ns
C
BMDCs
Pru
TN
NI
1h
2h
4h
6h
16h
6h
16h
KDa
130
140
37
25
37
65
50
IRE1α
P-PERK
PERK
P-eIF2α
CHOP
GAPDH
XBP1s
Tubulin
D
Flt3/Notch-cDC1
Pru
NI
2h
4h
6h
16h
IRE1α
XBP1s
PERK
P-eIF2α
CHOP
Tubulin

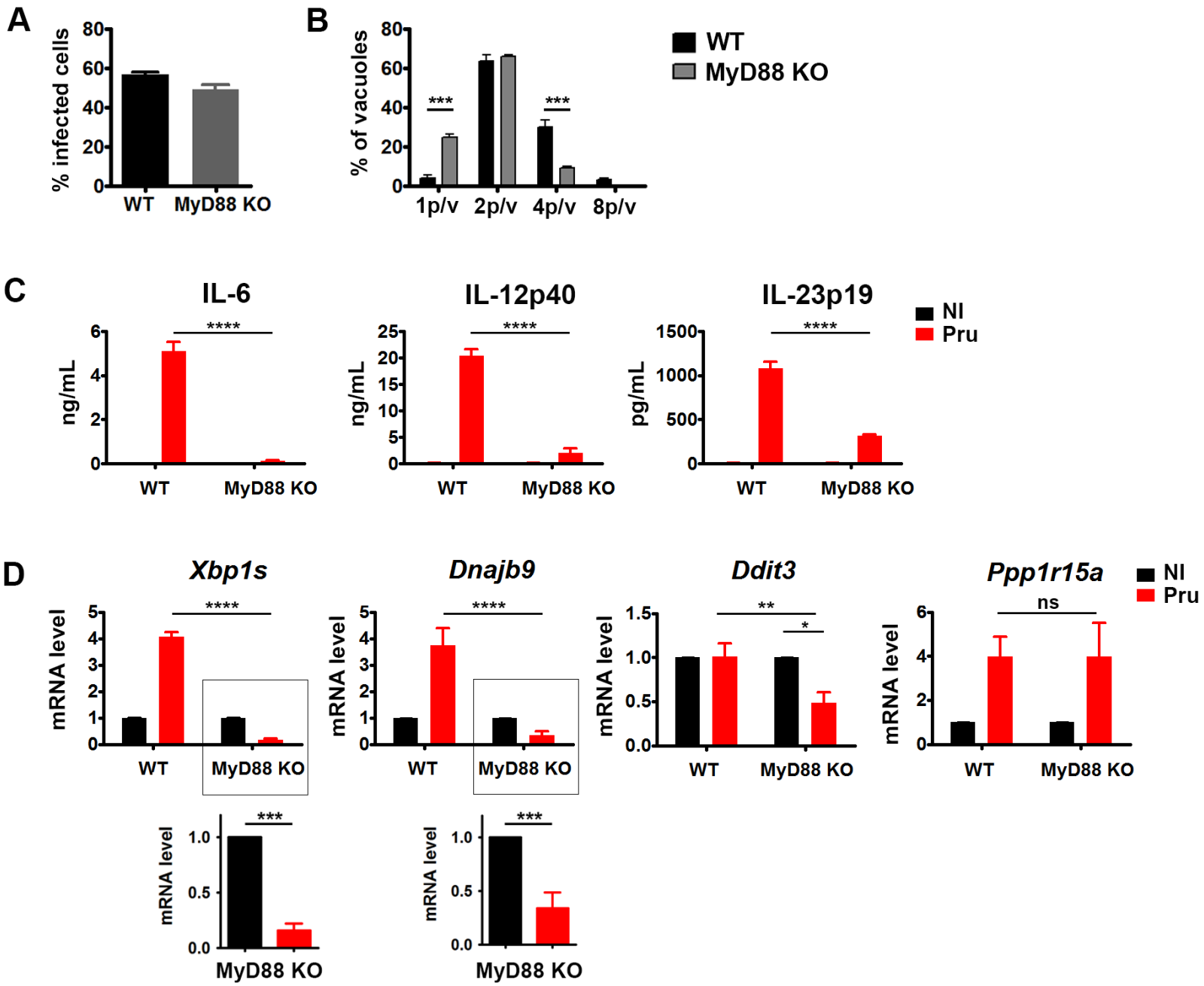
A
% infected cells
80
60
40
20
0
WT
MyD88 KO
B
% of vacuoles
80
60
40
20
0
***
***
1p/v
2p/v
4p/v
8p/v
WT
MyD88 KO
C
IL-6
ng/mL
6
4
2
0
****
WT
MyD88 KO
IL-12p40
ng/mL
25
20
15
10
5
0
****
WT
MyD88 KO
IL-23p19
pg/mL
1500
1000
500
0
****
WT
MyD88 KO
NI
Pru
D
Xbp1s
mRNA level
5
4
3
2
1
0
****
WT
MyD88 KO
Dnajb9
mRNA level
5
4
3
2
1
0
****
WT
MyD88 KO
Ddit3
mRNA level
1.5
1.0
0.5
0.0
**
*
WT
MyD88 KO
Ppp1r15a
mRNA level
6
4
2
0
ns
WT
MyD88 KO
NI
Pru
mRNA level
1.0
0.5
0.0
***
MyD88 KO
mRNA level
1.0
0.5
0.0
***
MyD88 KO

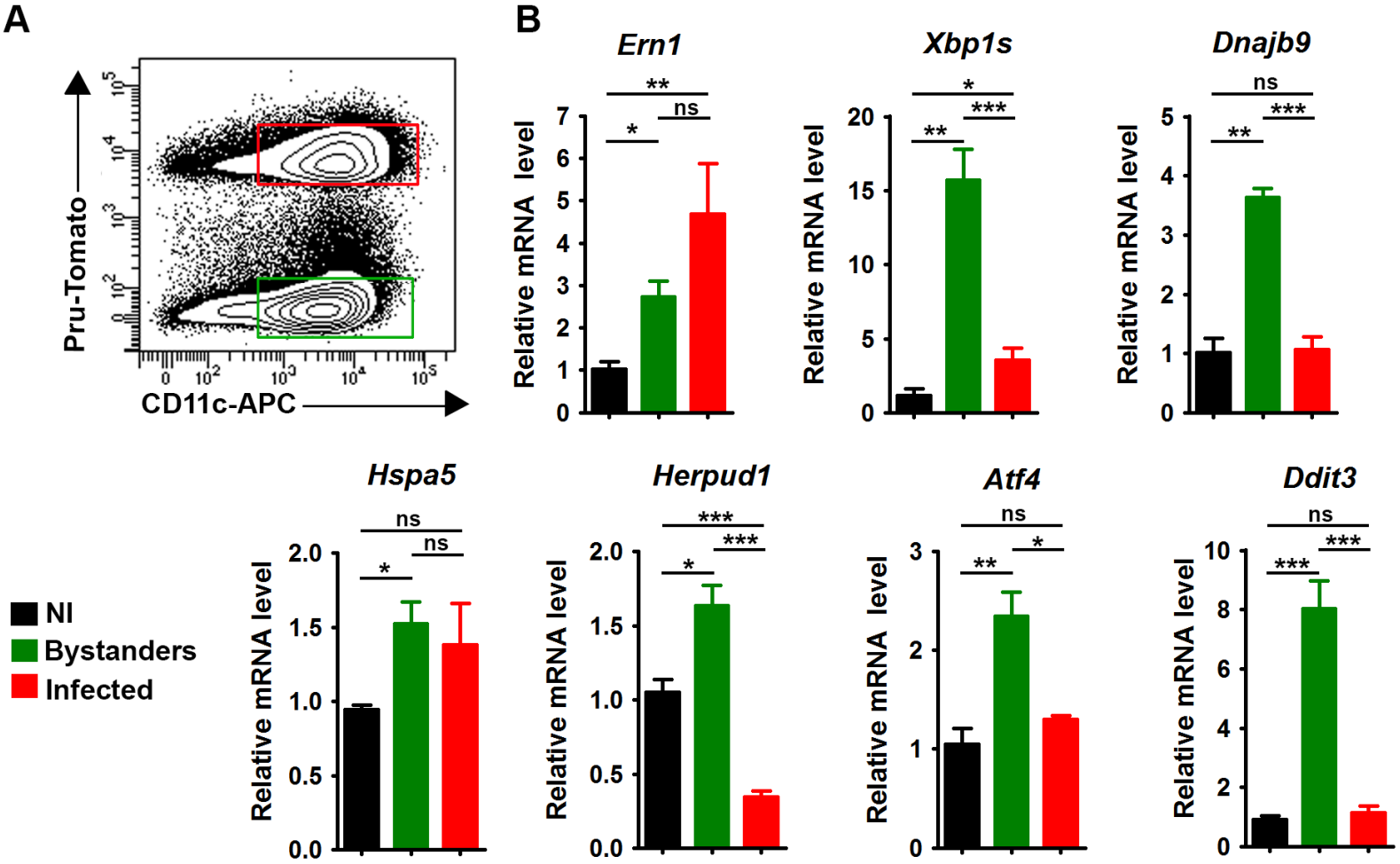
A
B
Pru-Tomato
CD11c-APC
Ern1
Xbp1s
Dnajb9
Hspa5
Herpud1
Atf4
Ddit3
Relative mRNA level
NI
Bystanders
Infected

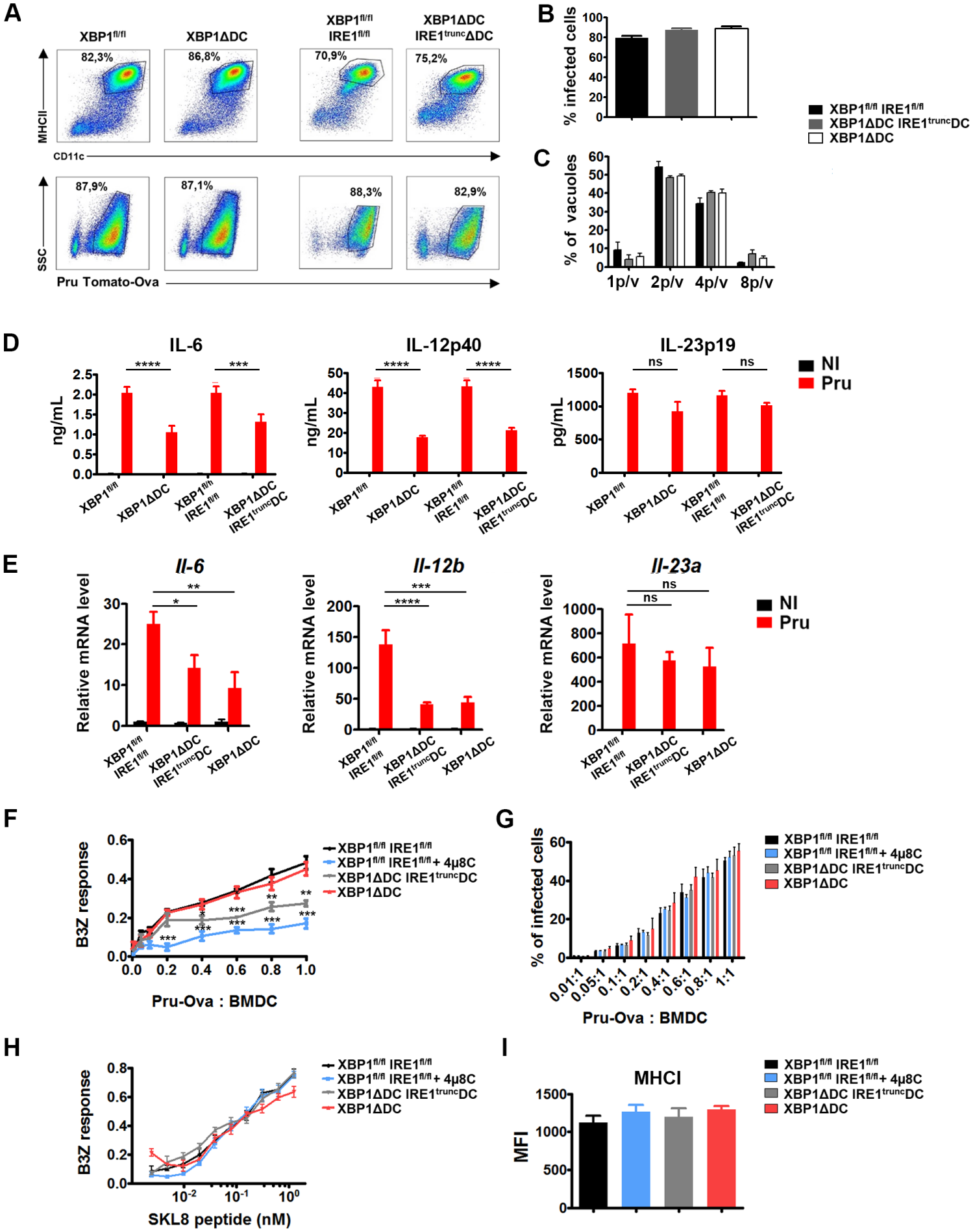
A
XBP1fl/fl
XBP1ΔDC
XBP1fl/fl IRE1fl/fl
XBP1ΔDC IRE1trunc ΔDC
82,3%
86,8%
70,9%
75,2%
MHCII
CD11c
87,9%
87,1%
88,3%
82,9%
SSC
Pru Tomato-Ova
B
% infected cells
XBP1fl/fl IRE1fl/fl
XBP1ΔDC IRE1trunc DC
XBP1ΔDC
C
% of vacuoles
1p/v
2p/v
4p/v
8p/v
D
IL-6
IL-12p40
IL-23p19
ng/mL
pg/mL
NI
Pru
ns
E
Il-6
Il-12b
Il-23a
Relative mRNA level
F
B3Z response
Pru-Ova : BMDC
XBP1fl/fl IRE1fl/fl + 4μ8C
G
% of infected cells
0.01:1
0.05:1
0.1:1
0.2:1
0.4:1
0.6:1
0.8:1
1:1
H
SKL8 peptide (nM)
I
MHCI
MFI

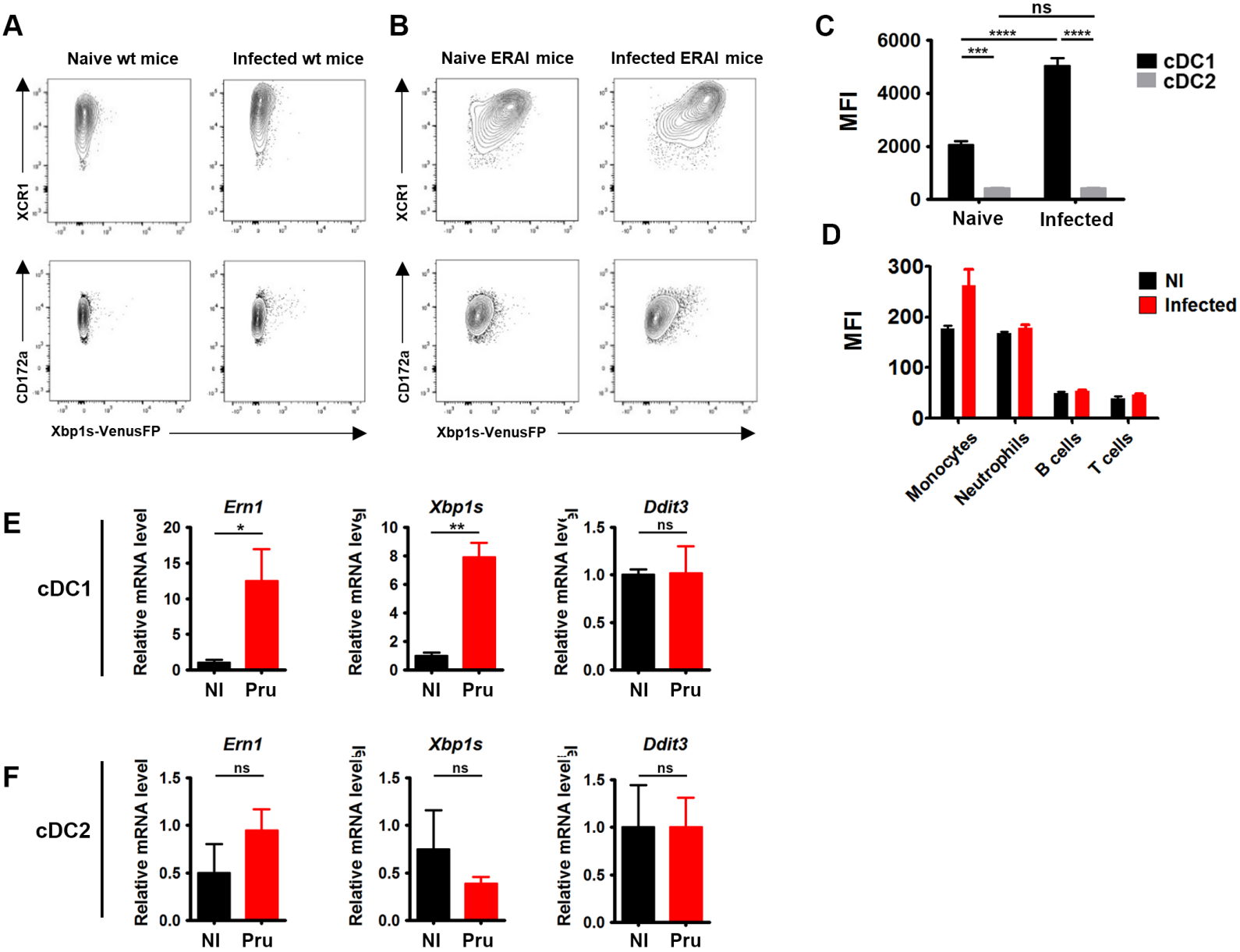
A
Naive wt mice
Infected wt mice
XCR1
CD172a
Xbp1s-VenusFP
B
Naive ERAI mice
Infected ERAI mice
XCR1
CD172a
Xbp1s-VenusFP
C
ns
****
****
***
6000
4000
2000
0
MFI
Naive
Infected
cDC1
cDC2
D
300
200
100
0
MFI
NI
Infected
Monocytes
Neutrophils
B cells
T cells
E
cDC1
Ern1
Xbp1s
Ddit3
Relative mRNA level
*
**
ns
NI
Pru
F
cDC2
Ern1
Xbp1s
Ddit3
Relative mRNA level
ns
NI
Pru

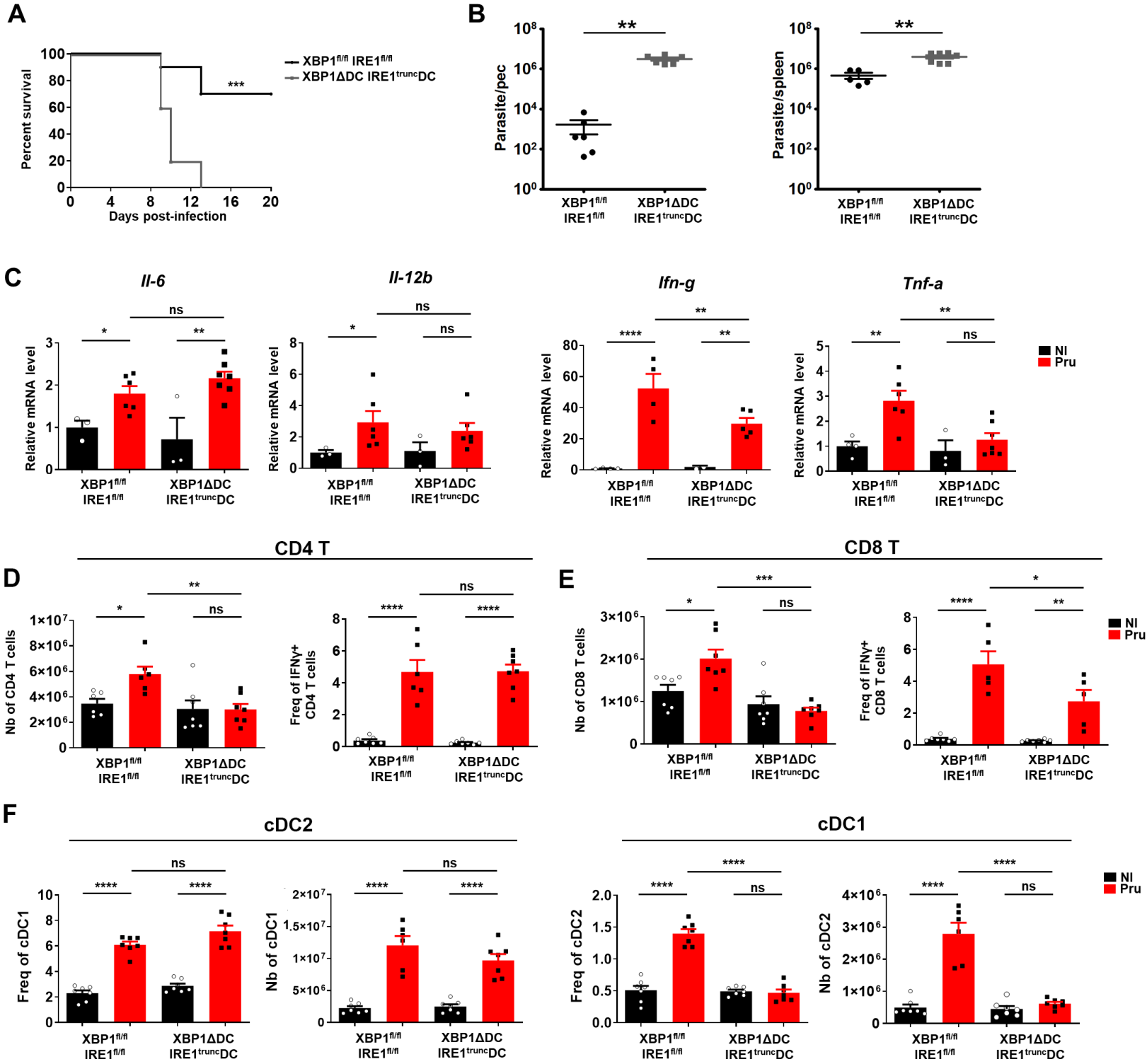
A
Percent survival
Days post-infection
XBP1fl/fl IRE1fl/fl
XBP1ΔDC IRE1trunc DC
***
B
Parasite/pec
Parasite/spleen
**
C
Il-6
Il-12b
Ifn-g
Tnf-a
Relative mRNA level
NI
Pru
D
CD4 T
Nb of CD4 T cells
Freq of IFNγ+ CD4 T cells
E
CD8 T
Nb of CD8 T cells
Freq of IFNγ+ CD8 T cells
F
cDC2
Freq of cDC1
Nb of cDC1
cDC1
Freq of cDC2
Nb of cDC2
ns

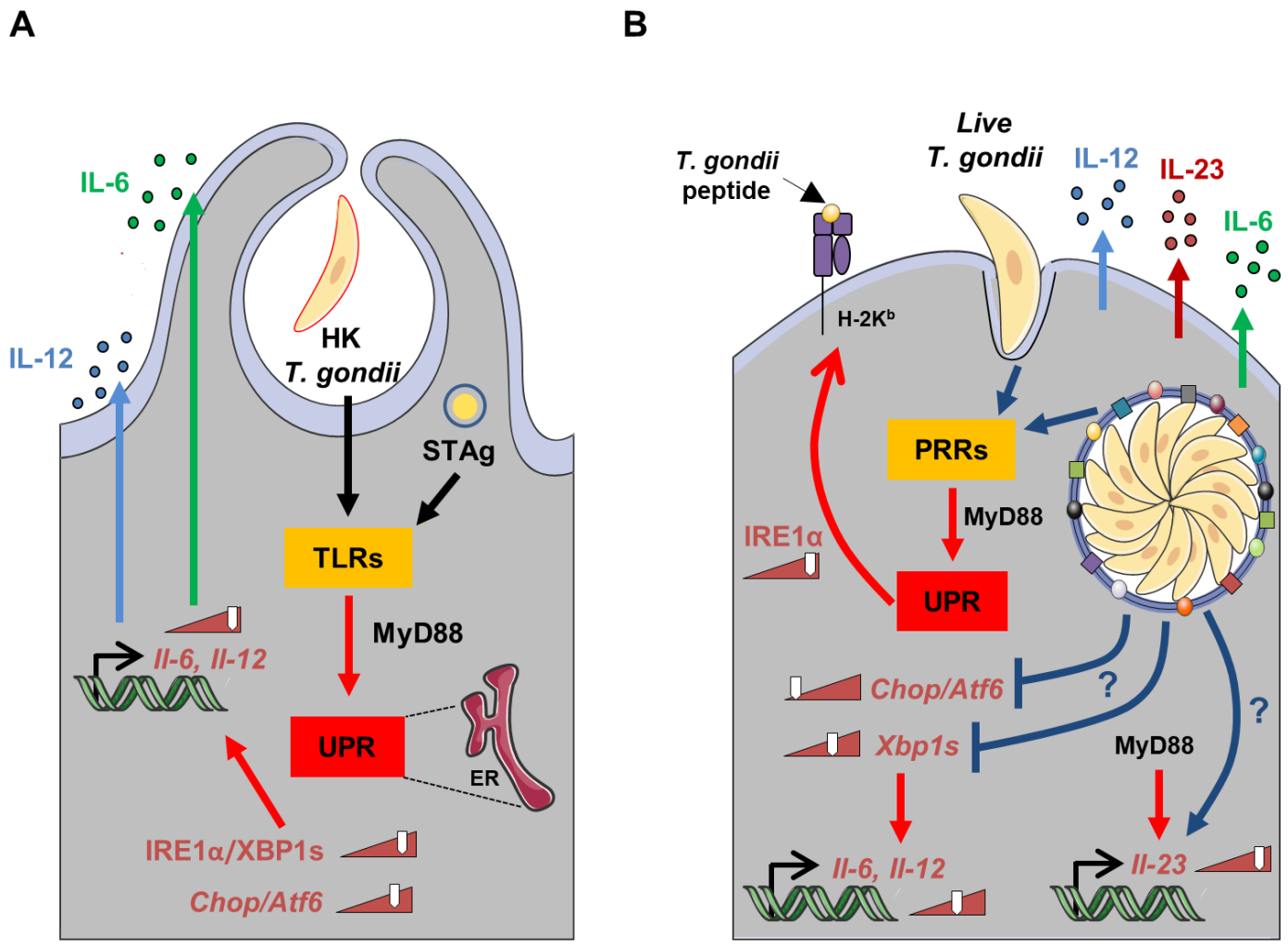
A
IL-6
IL-12
HK
T. gondii
STAg
TLRs
MyD88
UPR
ER
Il-6, Il-12
IRE1α/XBP1s
Chop/Atf6
B
T. gondii
peptide
Live
T. gondii
IL-12
IL-23
IL-6
H-2Kᵇ
PRRs
MyD88
IRE1α
UPR
Chop/Atf6
Xbp1s
?
?
MyD88
Il-6, Il-12
Il-23